Water properties and bottom water patterns in hadal trench environments

Jessica Kolbusz[1], Jan Zika[2], Charitha Pattiarachi[3] and Alan Jamieson[1]

[1]Minderoo-UWA Deep-Sea Research Centre, University of Western Australia, Crawley, 6009, Australia
[2]School of Mathematics and Statistics, University of New South Wales, Sydney, 2052, Australia
[3]Oceans Graduate School, University of Western Australia, Crawley, 6009, Australia

Correspondence to: Jessica L. Kolbusz (jess.kolbusz@uwa.edu.au)

Keywords

Antarctic Bottom Water, hadal, hadopelagic, Lower Circumpolar Deep Water, trench

Abstract

We examine baseline water properties and bottom water patterns in hadal trench environments across the Southern Ocean, Indian Ocean, and Western Pacific. Significant differences are identified in the South Fiji Basin and surrounding the Philippine Sea, primarily due to the movement of cold Lower Circumpolar Deep Water along topographic features, highlighting the importance of a trench's geospatial position. We present the first hydrographic profiles in the Java Trench, warranting further research. Salinity increases with increasing depth for profiles over 10,000 dbar, with potential causes including instrumentation error, internal mixing, and saline pore water expulsion. These hadopelagic variations are crucial for assessing climate change impacts, especially regarding Antarctic Bottom Water. The study underscores the importance of incorporating these adiabatic conditions for insights into ecological biodiversity, alongside the baseline conditions presented being indispensable for future oceanographic research across multiple disciplines.

1 Introduction

The oceanic hadal zone, regions where water depths are greater than 6,000 m, is located mainly in subduction trenches, fracture zones and a few deep basins (Jamieson & Stewart, 2021). This remote region of water is arguably the most understudied habitat in the marine environment (Webb et al., 2010). The most conspicuous geomorphological features of the hadal zone are the large subduction trenches in the Atlantic, Southern, Indian and, particularly, the Pacific Ocean (Jamieson, 2015). These trenches are characterised by extreme pressures, cold temperatures, no light penetration, frequent subduction earthquakes and geothermal heating of 0.05°C within waters of the same salinity (Jamieson et al., 2010; Taira et al., 2005; Oguri et al., 2013; Joyce et al., 1986). Of these 27 trenches, most exceed 8,000 m in depth, with four exceeding 10,000 m (Bongiovanni et al., 2021). Over 6,000 m, the volume is approximately 0.21% of the total ocean, however, it is 45% of the ocean's total depth range (Jamieson, 2015).

Sampling and exploration of the hadal benthic habitats have, in recent years, seen a renaissance (Jamieson, 2018), with biological data sets being obtained for multiple taxonomic groups from multiple depths over multiple trenches (Jamieson, Linley, et al., 2021; Jamieson & Linley, 2021; Swan et al., 2021; Weston & Jamieson, 2022). As these studies develop from simple species discovery and observations of presence/absence, other abiotic factors are required to explain larger-scale ecological patterns in vertical distribution and biogeography (Nunoura et al., 2016; Glud et al., 2013). For example, hadal benthic fauna are supported by the deposition of nutritious organic material from the surface ocean into the trench sediments (Ichino et al., 2015), increasing microbial activity and carbon accumulation through mass-wasting events or internal waves (Oguri et al., 2022; Turnewitsch et al., 2014; van Haren, 2020b). In addition, understanding these habitats' geomorphological structuring is valuable in explaining species' relationships with substrate (Stewart and Jamieson, 2018; Jamieson et al., 2022). While single point temperature and salinity measurements were made in multiple trenches in the 1950s and 60s (Belyaev, 1989), full-ocean-depth hydrographic profiles of conductivity (for salinity), temperature and depth (CTD) are rarely reported, excluding those surrounding the Izu-Bonin-Mariana Arc System, making inter-trench variation therein are seldom accounted for in observations (Stewart and Jamieson, 2018; Jamieson and Fujii, 2011).

The extrapolation of hydrographic conditions to a trench system's broader physical oceanographic context has been notably underrepresented in research. However, regional studies have provided insight into these depths but with some bias towards the *Challenger Deep* in the Mariana Trench (Greenaway et al., 2021; Mantyla and Reid, 1978; Taira et al., 2005; van Haren et al., 2017, 2021; Taira et al., 2004), and neighbouring trenches (Kawagucci et al., 2018; Taira, 2006). Long-term temperature sensor deployments have shown the impact of internal tidal waves and turbulent spurs due to warm waters pushed from above the trench on the de-stagnation of the water below 6000m. These examples of turbulent mixing, not accounting for horizontal advection, can potentially decrease stratification to a degree comparable to that of geothermal heating (convective turbulence) (van Haren, 2023). Considering this, turbulence can be ten times higher in the upper hadopelagic (6,500 – 8,500 m) compared to the bottom of the hadopelagic (10,300 – 10,850 m) (Huang et al., 2018). Additionally, local cyclonic circulation over trenches has been identified over the Philippine Trench (Zhai and Gu, 2020; Tian et al., 2021) and the Mariana Trench (Huang et al., 2018), with both circulation patterns informed by bottom water circulation.

In the broader context of the global overturning circulation, trenches may serve as conduits for the transport of dense bottom water masses. Temperature and salinity gradients drive the overturning circulation, which transports cool, dense water, formed around Antarctica (Antarctic Bottom Water, AABW) in the Weddell Sea, Ross Sea and Adélie Land (Zhang and Delworth, 2016; Talley, 2013a; Gordon, 1986b; Rintoul, 1985) as well as North Atlantic Deep Water (NADW), formed from dense overflows in the Nordic Seas, lower Labrador Sea Water and recirculating AABW, to fill the ocean basins (Gordon, 1986a; Dickson and Brown, 1994; Orsi et al., 1999). The cool water eventually rises, and is heated, flowing poleward to replace denser water, creating a global cell of circulation (Stommel and Arons, 1959). Diapycnal exchanges also play an important role in modifying pathways and ventilation timescales (Cimoli et al., 2023). However, the full implication of these findings and how they play into the variation in trench conditions is yet to be understood on an inter-basin scale.

The Southern Ocean plays a significant role in the deep overturning circulation in AABW formation and its influence on NADW production and cell closure (Rahmstorf and England, 1997; Goodman, 1998; Sloyan and Rintoul, 2001). This lower limb of the overturning circulation fills the abyssal basins of the Atlantic, Indian and Pacific Oceans (Orsi et al., 1999, 1993; Mantyla and Reid, 1995). AABW upwells locally as it moves northwards, making it the primary volumetric source of deep water in the Pacific and Indian Oceans, with no high-salinity water source to the north (Talley, 2011). These patterns of sinking and spreading through the world's oceans have been captured in observations (Wust, 1933) and are considered a key component of climate regulation (Naveira Garabato et al., 2017; Schmitz, 1995).

In the Pacific Ocean, Lower Circumpolar Deep Water (LCDW) mostly comprises of AABW and remnant NADW from the Southern Ocean (Johnson, 2008; Orsi et al., 1999). LCDW flows northward on the western side of the Southwest Pacific Basin, the Tonga-Kermadec Ridge (TKR), and reaches the Samoan Passage near the northern end of the Tonga Trench (Roemmich et al., 1996; Taft et al., 1991). The TKR prevents abyssal water from entering the South Fiji Basin; therefore bottom waters are formed by the densest parts of the Upper Circumpolar Deep Water (UCDW) entering the New Hebrides Basin via the entrance to the southern Solomon Sea Basin (Germineaud et al., 2021; Kawabe and Fujio, 2010).

Just north of the Samoan Passage, the LCDW bifurcates into a western and eastern branch driven by the complex topography in the region (Kawabe et al., 2003). The western branch flows north-westward, arriving in the East Mariana Basin where it separates into East Caroline Basin to the south and north, and is transported to the Izu-Ogasawara Trench followed by the Japan Trench (Fujio et al., 2000; Fujio, 2005; Siedler et al., 2004). A portion of the LCDW reaches the south of the Mariana Trench, the Yap-Mariana Junction from the northward flow (Kawabe and Fujio, 2010), where it flows into the northern and southern Yap Trench and partially into the Philippine Basin (Liu, 2022; Liu et al., 2020; Zhai and Gu, 2020). The Yap Ridge then blocks the circulation of water, causing it to enter the Western Caroline Basin, where it can enter the Palau Trench (Zhai and Gu, 2020; Liu, 2022). Modelling suggests that the bottom layers of the Philippine Basin form an anticyclonic gyre in the south and two cyclonic gyres in the northeast and northwest, followed by possible cyclonic circulation over the Philippine Trench (Zhai and Gu, 2020).

AABW dominates bottom waters in the Indian Ocean as it enters through two pathways and is observed as far north as 12°N in the Bay of Bengal (Chinni et al., 2019; Singh et al., 2012). Firstly, it enters through the Enderby Basin, forming in the Weddell Sea (Orsi et al., 1999). Secondly, through the Australian-Antarctic Basin, where the bottom water was originally formed from the Adélie Land and the Ross Sea (Rintoul, 1985; Mantyla and Reid, 1995). Elevated dissipation rates from tidal mixing and current fluctuations in the Indian Ocean contribute to a higher ventilation rate of deep and bottom water in the Indian Ocean compared to the Pacific and Atlantic Oceans (Fine et al., 2008). The deep waters of the Indian ocean, similarly to in the Pacific Ocean, are sourced primarily from upwelled bottom waters, which are then heated and, through diapycnal transformation, returned to the sea surface, and are cooled and recycled back into AABW in the Southern Ocean (Talley, 2013a).

In this paper, we explore twelve hadal trenches using full-ocean-depth CTD profiles derived from free-fall landers to unravel the complexities of the trenches and the interplay between the hadopelagic and global circulation patterns of bottom waters.

The World Ocean Circulation Experiment (WOCE) measured vertical sections along each hydrographic line covering the globe in the late 1980s and early 2000s, with some repeat sections now part of the Global Ocean Ship-Based Hydrographic Investigations Program (GO-SHIP) (Koltermann et al., 2011; Orsi and Whitworth, 2005; Talley, 2007, 2013b; Sloyan et al., 2019). Measurements were restricted to 6000 m, although global transport estimates were substantial for climate studies (Ganachaud, 2003; Ganachaud and Wunsch, 2000). We aim to gain insights into hadal trench connections with the abyssal waters above by analysing the opportunistic full-ocean-depth CTD data sets and repeat GO-SHIP global observations. Through this analysis, we describe physical oceanographic conditions within the hadal trenches of the Southern Ocean, Indian Ocean and Pacific Ocean, spanning seven of the ten hadal provinces (Watling et al., 2013). Furthermore, we link changes in water properties in the western Pacific Ocean to AABW and LCDW source waters to enhance our understanding of the physical oceanographic conditions which shape ecosystem survival in these unique environments.

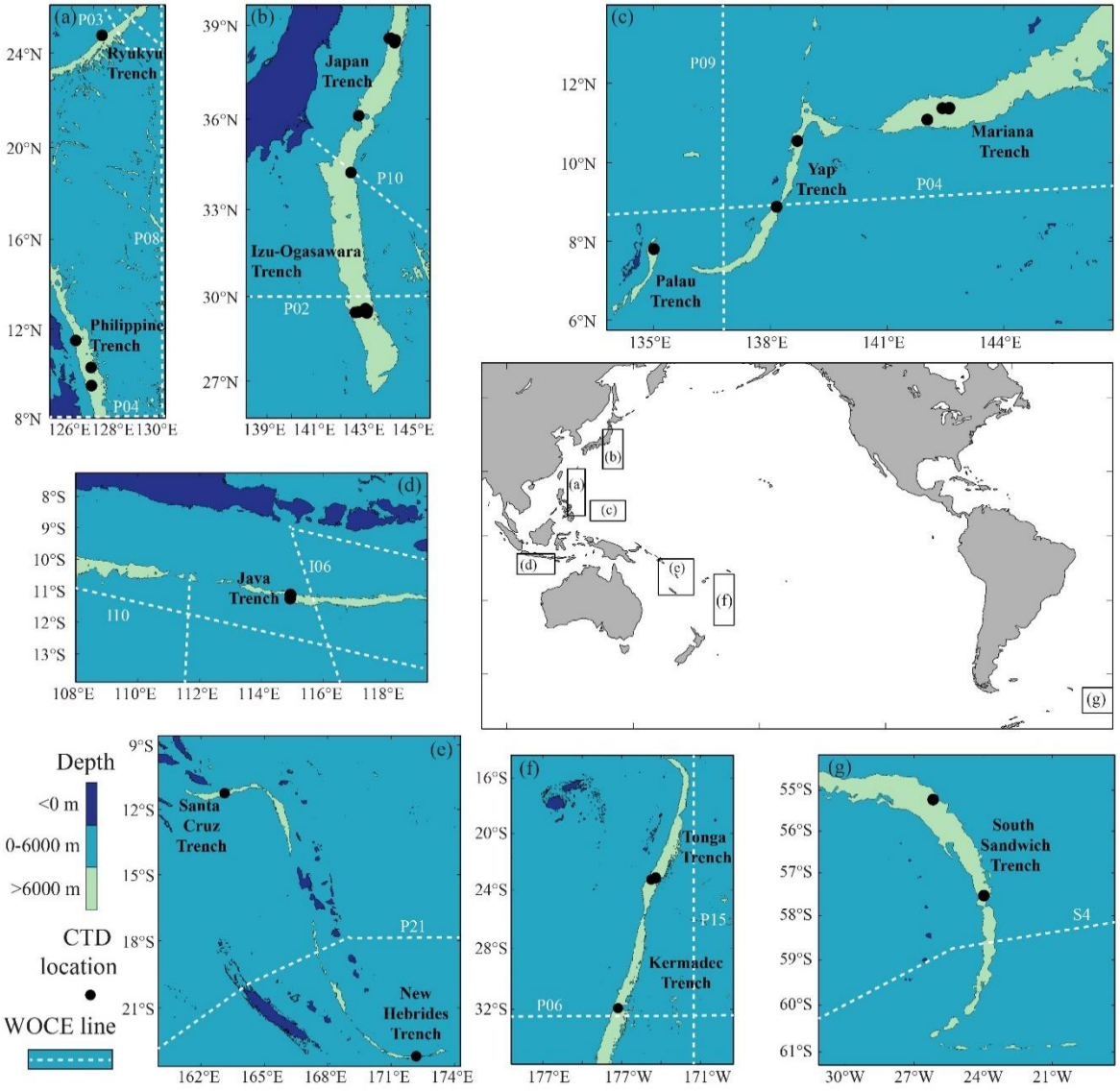

Figure 1. Geographic locations of the hadal trenches used in this study, including CTD deployment locations marked in black. (a) Ryukyu Trench and Philippine Trench; (b) Japan Trench and Izu-Ogasawara Trench; (c) Palau Trench, Yap Trench, and Mariana Trench; (d) Java Trench Ć Santa Cruz Trench and New Hebrides Trench; (f) Tonga Trench and Kermadec Trench and (g) South Sandwich Trench. Individual deployment details are provided in Table S1. Bathymetric details and features are provided in Table S1. Ocean elevation data was sourced from the GEBCO Compilation Group (2021) and reproduced using m_map in MATLAB (Pawlowicz 2020).

2 Methods

We define the hadal water properties and bottom conditions of twelve of the world's hadal trenches spanning three oceans and seven hadal biogeographic provinces (Belyaev, 1989; Watling et al., 2013) (Table 1). Full-ocean-depth landers mounted with

CTDs were deployed between 2018 and 2022. The deployment locations, relevant features, and nearby repeat hydrography sections (both World Ocean Circulation Experiment (WOCE) and Global Ocean Ship-Based Hydrographic Investigations Program (GO-SHIP)) used throughout the paper are indicated in Figure 1 and Table 1 (Orsi and Whitworth, 2005; Talley, 2007, 2013b; Sloyan et al., 2019). The location of features mentioned, other than the trenches are found in Figure S1. Quality control and analysis are detailed in the following section, producing 33 CTD profiles in total (Figure 1, Table 1, Table S1).

2.1 Study sites

In the Southern Ocean, deployments were made in the South Sandwich Trench (SAND) (~55˚S / 23˚W) to 8,266 m. SAND falls within the Southern Antilles hadal province (Watling et al., 2013). Bottom circulation in the region is promoted by the Weddell Gyre exporting of newly formed dense Weddell Sea Bottom Water, or Antarctic Bottom Water (AABW), northward through the Scotia Sea and along the South Sandwich Trench through the steep slopes inducing strong downwelling (Zhang and Delworth, 2016).

The deepest point of the Indian Ocean is the Java Trench (JAV), where deployments were made to 7,178 m (11˚S / 115˚E). Bottom water (modified AABW and LCDW) reaches the Java Trench from the West Australian Basin to the south (Mantyla and Reid, 1995; Sloyan, 2006; Arvapalli. et al., 2022).

The Kermadec Trench connects at the southern end of the Tonga Trench within the same convergence system in the central south Pacific, separated only by the subducting Osborn Seamount (Jamieson et al., 2020). Deployments were made in the Tonga Trench (~23˚S / 174˚W) to a maximum depth of 10,823 m, and 9,986 m and in the Kermadec Trench (~32˚S / 177˚E). Bottom circulation in the region is dominated by the major AABW/LCDW pathway into the Pacific, which enters from the south along the Tonga-Kermadec Ridge and flows north (Warren, 1981; Kawabe, 1993; Taft et al., 1991; Purkey et al., 2019). Surrounding the Solomon Sea lies the Bougainville-New Hebrides hadal province, where deployments were made to 7,770 m in the New Hebrides Trench (23˚S / 172 ˚E) and 9,125 m in the Santa Cruz Trench (11˚S / 163 ˚E). Bottom water masses in these trenches are akin to Upper Circumpolar Deep Water (UCDW) which have entered the Solomon Sea from the north (Germineaud et al., 2021).

In the central northwest Pacific Ocean, deployments were completed to a maximum of 10,925 m in the Mariana Trench (MAR) (~11˚N / 142˚E); 8,885 m in the Yap Trench (YAP) (~9˚N / 138˚E); 8,000 m in the Palau Trench (PAL) (~8˚N / 135˚E), and, 10,007 m in the Philippine Trench (PHI) (~10˚N / 126˚E). Further north, there were deployments to 9,767 m in the Izu Ogasawara Trench (IOT) (29˚N / 142˚E) and to 8,004 m in the Japan Trench (JPT) (36˚N / 143˚E). These deployments span three hadal provinces (Table 1). Bottom water circulation in this region is driven by AABW/LCDW, which enters the east of the Mariana Basin in the North Pacific (Kawabe et al., 2003; Siedler et al., 2004). The westward component propagates through MAR, flowing through the westernmost end and over the YAP and PAL trenches (Kawabe and Fujio, 2010). The northern branch flows through the Wake Island Passage and along the Izu-Ogasawara Ridge, filling IOT and JPT (Tian et al., 2021). The Philippine hadal province has a unique location west of the Philippine Basin, not immediately near the primary bottom water circulation of the Pacific Ocean (Kawabe and Fujio, 2010). Deep bottom circulation along the trench consists of

southward and northward currents on the western and eastern slopes of the trench, respectively (Zhai and Gu, 2020), which is not unlike other local cyclonic circulation observed in other trenches (Huang et al., 2018). This deep water mass is likely well-transformed AABW/LCDW that fills the Philippine Sea from the north (Wang et al., 2017; Kawabe and Fujio, 2010; Tian et al., 2021).

155

Table 1. Summary of the hadal lander deployments from RV Pressure Drop used in this study. Specific deployment details in Table S1.

Trench	**Hadal Province (Belyaev, 1989; Watling et al., 2013)**	**# Profiles**	**Date**	**Depth range (m)**	**Repeat hydrography section within ±6° longitude and ±4° latitude**
South Sandwich Trench (SAND)	Southern Antilles	2	February 2019	8,071-8,254	S4 (WOCE)
Java Trench, or Sunda Trench (JAV)	Java	3	April 2019	6,136-7,197	I10 (GO-SHIP), I06 (WOCE)
Kermadec Trench (KRT)	Tonga-Kermadec	1	December 2021	9,978	P06 (GO-SHIP)
Tonga Trench (TON)	Tonga-Kermadec	2	June 2019	7,471-10,811	P15 (GO-SHIP)
New-Hebrides Trench (NHT)	Bougainville-New Hebrides	1	December 2021	7,960	P21 (WOCE)
Santa Cruz Trench (SCZ)	Bougainville-New Hebrides	1	December 2021	9,370	P21 (WOCE)
Mariana Trench (MAR)	Mariana	5	April 2019 and June 2020	7,495 – 10,922	P04 (GO-SHIP)
Yap Trench (YAP)	Mariana	2	July 2022	5,981 – 8,885	P04 (GO-SHIP), P09 (GO-SHIP)
Palau Trench (PAL)	Mariana	1	July 2022	7,995	P04 (GO-SHIP), P09 (GO-SHIP)
Philippine Trench (PHT)	Philippine	3	February 2021	6,995- 10,058	P04 (GO-SHIP), P08 (GO-SHIP)
Izu-Ogasawara Trench (IOT)	Aleutian- Japan	6	August 2022	6,462 – 9,752	P02 (GO-SHIP), P09 (GO-SHIP)
Japan Trench (JPT)	Aleutian- Japan	5	September 2022	6,462 – 7,991	P10 (GO-SHIP), P09 (GO-SHIP)

2.2 Data collection

The hydrographic CTD profiles were collected as part of the *Five Deeps Expedition* and the follow-on *Ring of Fire Expedition* (2020-2022), on the RV *Pressure Drop*. To support the diving operations of the full-ocean-depth submersible DSSV *Limiting Factor*, and collect scientific data (e.g. Jamieson et al., 2021), three hadal landers were used in unison (known as *Skaff, Flere* and *Closp*). The landers were equipped with CTD probes (SBE 49 FastCAT; SeaBird Electronics, Bellevue, US) that, during both the descent and ascent, recorded conductivity, temperature, and pressure at 10-second intervals. The CTDs measured conductivity, temperature and pressure at ± 0.0003 S/m, ±0.002ºC and ±0.1% of the full-scale range, respectively (Sea-Bird Scientific, 2020).

The landers were released from the ship and descended until reaching the seafloor, where they performed autonomous filming operations for several hours before their ascent was initiated by jettisoning ballast weights via acoustic command. The landers descended at an average speed of 0.6 $ms^{-1,}$ and the design did not require any corrections for ship motions in CTD casts.

2.3 Data processing

The CTD data were processed using the standard procedures incorporated within the SBE Data Processing Software (Sea-Bird Scientific, 2018). Automated processing including aligning the temperature and conductivity data in time relative to the pressure and cell thermal mass corrections occurred within the sensor (Sea-Bird Scientific, 2020). A Wild Edit flagged data outside two standard deviations away from the mean. This was followed by applying a median filter to remove spikes. These methods were completed as recommended by Seabird. Profiles were discarded if Wild Edit bad flags were greater than 20% of the profile or if other lander-related situations occurred, influencing the data, and making the profile unusable. Post-cruise calibrations were carried out, as recommended by SeaBird and post-corrections were made using offset correction coefficients. Absolute salinity (S_A, g kg^{-1}), Conservative Temperature (Θ) and Potential Density referenced to 6000 dbar (σ_6) were calculated using the Gibbs-SeaWater (GSW) software which defines the thermodynamic properties of seawater based on a Gibbs function formulation as recommended by IOC (IOC et al., 2010). Then, the down-cast profiles were averaged to 10 dbar bins with the first 50 dbar of the water column removed due to lander effects and a gaussian filter applied.

A conservative approach was taken with the data due to limited profiles and possible limitations, including the drift of conductivity measurements in SBE CTDs, (van Haren et al. 2017; Goretski et al. 2022). Therefore, if there was a GO-SHIP station deeper than 4500 dbar, taken within ±4 years of the lander deployment and lying within ±6° longitude and ±4° latitude of its location, a salinity offset from the closest station was applied to the CTD data. Using the stable portion of the water column at the highest pressure, the S_A was adjusted after conversion from the Practical Salinity in the GO-SHIP data at the same Θ and pressure (Supplementary 3). In total, 33 CTD profiles were used (Figure 1).

2.3 Data analysis

We derive the comparative mean water conditions together with Θ-S_A plots and apply a source water type analysis. Through these mechanisms we are addressing the heterogeneity of trenches. The downcast profiles were used to eliminate the potential heating effects generated by illumination devices on the landers. Only profiles measuring to over 6000 dbar were considered in this study. Despite our focus being on the hadopelagic (> 6000 dbar), measurements within abyssal waters between 4000 and 6000 dbar are included in the figures and used in conjunction with repeat hydrographic sections for baseline and temporal and spatial comparisons (Figure 1, Table 1). All WOCE and continued GO-SHIP lines within ±6° longitude and ±4° latitude of the deployment locations were plotted alongside our deployments after being downloaded from the CCHDO (CLIVAR and Carbon Hydrographic Data Office https://cchdo.ucsd.edu/). Θ-S_A plots, derived initially by Helland-Hansan (1916), were then plotted along isopycnals referenced to 6000 dbar (Pond and Pickard, 1983). This reference pressure was adopted given the depths of the profiles (> 6000 dbar), therefore more accurately reflecting the thermodynamic properties of deep-water masses. The mean in-situ Temperature, T, Θ and S_A at 7000 m were calculated in each trench for comparison since the Java Trench is the shallowest included within this study at 7192 m (Bongiovanni et al., 2021). A Θ-S_A plot of bottom conditions in the trenches was also generated for comparative purposes.

We apply a source water type analysis to the profiles along the western Pacific, likely containing Antarctic Bottom Water (AABW) and Lower Circumpolar Deep Water (LCDW) to understand the broad spatial differences. Restrictions on using basic Optimum multiparameter analysis (OMP) at a basin scale meant that mixing, including biogeochemical processes, cannot be ignored (Karstensen and Tomczak, 1998; Leffanue and Tomczak, 2004), and in our instance, we were limited to the conservative parameters of temperature and salinity. Weightings from 1-1, 5-1 and 10-1 for Θ-S_A were tested, however the difference in the resulting fractions was <0.0001, hence we omitted using weightings and considered 1-1. Additionally, we did not include a non-negativity constraint as our results contained no non-negative values. With these considerations in mind, the analysis can be formulated as a simple end-member mixing in Θ-S_A space. Trenches included were KRT, TON, MAR, YAP, PAL, PHI, IOT and JPT. The source water types of AABW and LCDW were defined along neutral density isopycnals, γ_n > 28.2 kg m^{-3} and 28.0 γ_n < 28.2 kg $m^{-3,}$ respectively (Table 2), at 60°S along the World Ocean Circulation Experiment P15 line (Figure 1) (Tamsitt et al., 2018; Abernathey et al., 2016; Solodoch et al., 2022).

We categorize the observations of Conservative Temperature (Θ_{Obs}) and Absolute Salinity (S_{Obs}) as being a mixture of two source water masses, AABW and LCDW. To estimate the fractional contributions of these two source waters (x_{AABW} and x_{LCDW} both between 0 and 1) we seek a solution to the following equations, inspired by classical OMP analysis (Tomczak, 1999; Tomczak and Large, 1989).

$$x_{AABW}\Theta_{AABW} + x_{LCDW}\Theta_{LCDW} = \Theta_{Obs}$$

$$x_{AABW}S_{A_{AABW}} + x_{LCDW}S_{A_{LCDW}} = S_{A_{Obs}}$$

$$x_{AABW} + x_{LCDW} = 1$$

We solve for x_{AABW} and x_{LCDW} for each observation by performing matrix left division in MATLAB. As the fractions were constrained to total 1, only the AABW fraction is reported in the results. To account for uncertainty in the source water properties the procedure was repeated for four combinations of maximum and minimum bounds of AABW and LCDW Θ and S_A (Table 3).

Table 2. Source water type values calculated from WOCE section P15.

	Conservative Temperature (Θ) °C	**Absolute Salinity (S_A) g kg^{-1}**
AABW$_{min}$	0.1115	34.8645
AABW$_{max}$	0.1119	34.8639
LCDW$_{min}$	1.2812	34.8863
LCDW$_{max}$	1.4526	34.8993

Table 3. Source water type combinations used to get the range uncertainty in the calculated source water type values defined in Table 2.

	Source water type combination
SWT1	AABW$_{min}$ and LCDW$_{min}$
SWT2	AABW$_{min}$ and LCDW$_{max}$
SWT3	AABW$_{max}$ and LCDW$_{min}$
SWT4	AABW$_{max}$ and LCDW$_{max}$

3 Results

The full-ocean-depth CTD profiles were limited to those over 6000 dbar and included in-situ temperature (T), practical salinity (S_P) and pressure (P). From these, Conservative Temperature (Θ) and Absolute Salinity (S_A) from the 12 hadal trenches were analysed to describe the conditions in the trenches within the trench sill and bottom conditions. Interpretation of Θ-S_A plots for each study region, including associated WOCE and GO-SHIP data over 4500 dbar were plotted, and additional source water type analysis was completed for the Northwest Pacific. The Θ and S_A profiles over pressure are provided in the supplementary information (Figures S4 to S11).

3.1 Water Properties

In the southernmost trench, the South Sandwich Trench (SAND), the hadal water mass characteristics were similar between the two deployments despite being 2º of latitude apart (Figure 1). From 6000 dbar to the seafloor, Θ decreased by at a rate of

-0.0145ºC/1000 dbar, while S_A had negligible vertical variation with dS_A/dp at 5.35×10^{-4} g kg^{-1}/1000 dbar (Figure 2). The GO-SHIP section, S4, decreased monotonically in Θ and S_A over depth, reaching a cooler bottom temperature of -0.76ºC.

In the Java Trench, otherwise known as the Sunda Trench, the average dΘ/dp was -0.009ºC/1000 dbar, and dS_A/dp was 0.0014 g kg^{-1}/1000 dbar between 6000 dbar and the seafloor (7360 dbar) (Figure 3). There is a more rapid increase toward the seafloor, also evident in section I06.

The profiles near TON and KRT decrease monotonically in Θ at a rate of -0.0095ºC/1000 dbar and 0.0015 g kg^{-1}/1000 dbar from 6000 dbar to the seafloor. The profile from KRT is consistent with P06 stations nearby; however, there is an increase in S_A of 0.002 g kg^{-1} in the bottom 1000 dbar of the trench (Figure 4b). Two of the profiles from TON indicate a similar increase in S_A at the bottom 1000 dbar of 0.015 g kg^{-1}. The remaining profile increases slightly in S_A (0.001 g kg^{-1}), following P15 more closely; however, it reaches only 6800 dbar (Figure 4a). The abyssal depths of WOCE sections P06 and P15 passing near TON and KRT are discussed extensively in the literature (Katsumata and Fukasawa, 2011; Macdonald et al., 2009).

In the New Hebrides Trench (NHT), dΘ/dp was 2.1×10^{-4} ºC/1000 dbar and dS_A/dp was 2.4×10^{-4} g kg^{-1}/1000 dbar between 6000 and the seafloor (7940 dbar). The rate of change was marginally different in the Santa Cruz Trench (SCZ). DΘ/dp was -3.7×10^{-4} ºC/1000 dbar and dS_A/dp was 2×10^{-4} g kg^{-1}/1000 dbar between 6000 and the seafloor (9350 dbar) (Figure 5).

In the Palau Trench (PAL), dΘ/dp was -0.003ºC/1000 dbar and dS_A/dp was 2.5×10^{-4} g kg^{-1}/1000 dbar between 6000 and the seafloor (8190 dbar) (Figure 6a). In the Yap Trench (YAP) the average rate of change in Θ was -0.015ºC/1000 dbar and dS_A/dp was -0.001 g kg^{-1}/1000 dbar between 6000 and the seafloor (8190 dbar). The two YAP profiles diverge in S_A at 5200 dbar with the deeper and more northern profile increasing in S_A at a greater rate into the trench (Figure 6). In the Mariana Trench (MAR), dΘ/dp is -0.002 ºC/1000 dbar between 6000 dbar and the seafloor (~11240 dbar). The rate of change of S_A is 0.0011 g kg^{-1}/1000 dbar); however, the rate doubled for over 8500 dbar at 0.0024 g kg^{-1}/1000 dbar for the four profiles exceeding 10500 dbar (Figure 6b).

The profiles in the Izu-Ogasawara Trench, dΘ/dp was -0.004ºC/1000 dbar and dS_A /dp was 2.7×10^{-4} g kg^{-1}/1000 dbar between 6000 and the seafloor (maximum of 10010 dbar) (Figure 7a). The rate of increase in S_A over 8500 dbar tripled for the deepest profile to 8.3×10^{-4} g kg^{-1}. In the Japan Trench (JPT), dΘ/dp was -0.0047ºC/1000 dbar, and dS_A/dp was -1.6×10^{-4} g kg^{-1}/1000 dbar between 6000 and the seafloor (maximum of 8170 dbar) (Figure 7a).

In the Philippine Trench (PHI), dΘ/dp was -0.003ºC/1000 dbar, and dS_A/dp was 1.7×10^{-4} g kg^{-1}/1000 dbar between 6000 and the seafloor (maximum of 10340 dbar) (Figure 8a). The rate of increase in S_A over 8500 dbar increased six-fold to 0.0011 g kg^{-1}/1000 dbar for the deepest profile (Figure 8b).

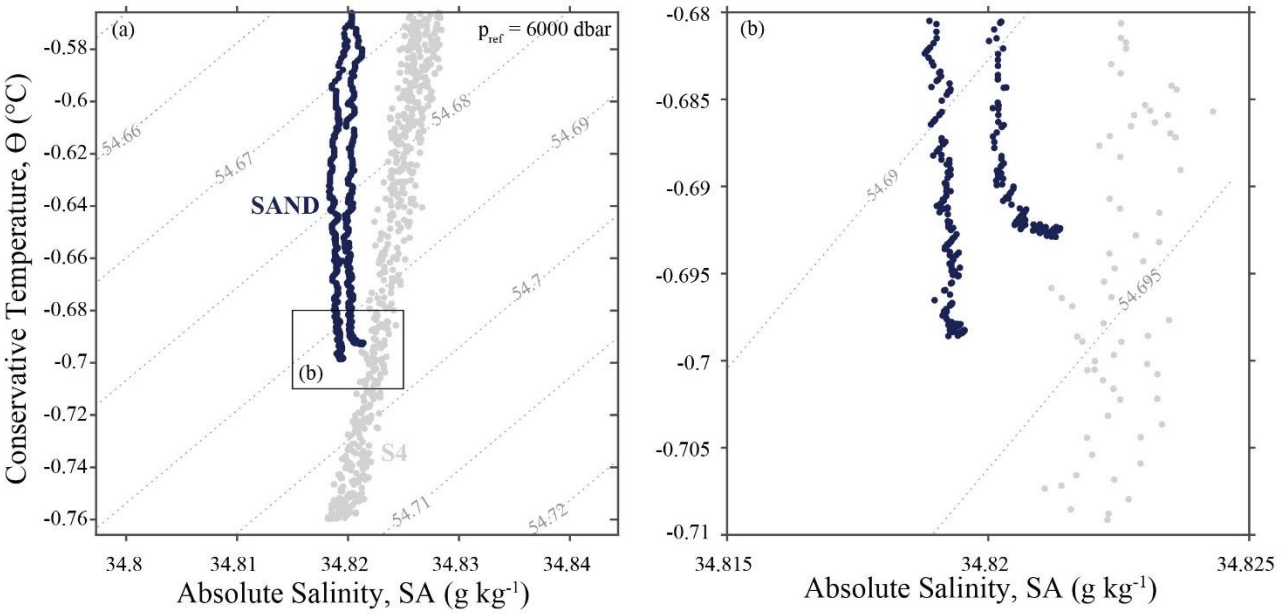

Figure 2. Θ-SA plots for the South Sandwich Trench (SAND) (a) over 4000 dbar (b) bottom waters. The rectangle in (a) shows the extent of (b). Isopycnals (contour lines) show the potential density referenced to 6000 dbar. The grey data points are WOCE section S4.

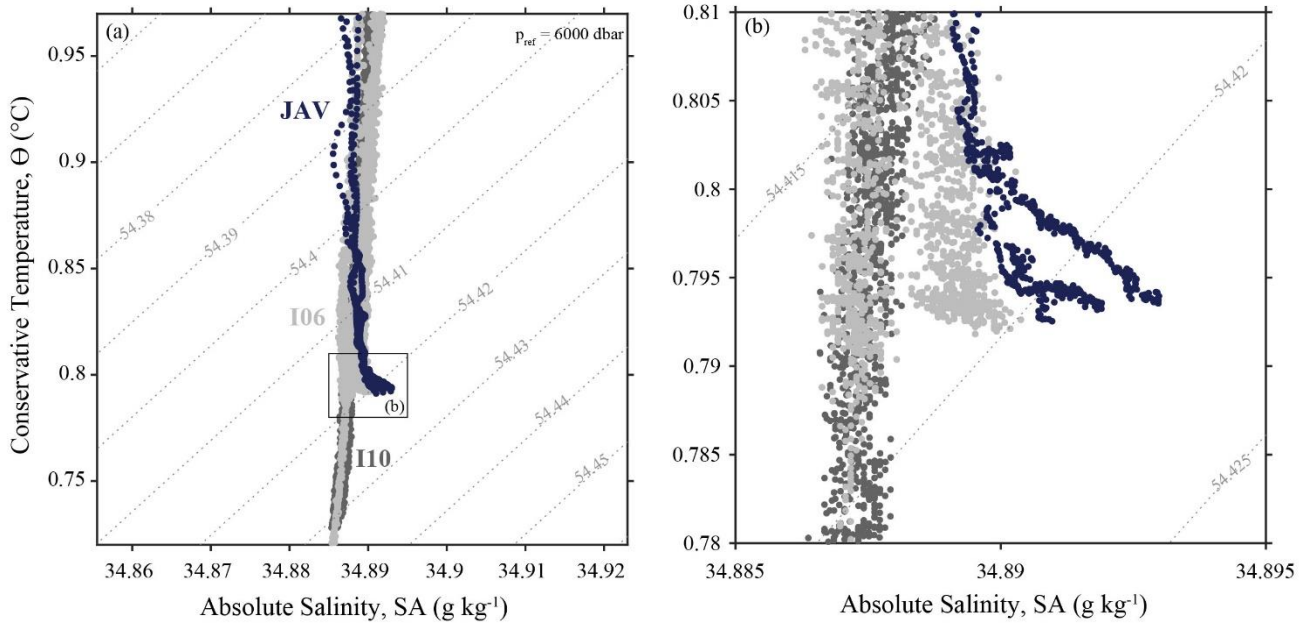

Figure 3. As in Figure 2 for the Java Trench. The grey is WOCE section I06 and I10.

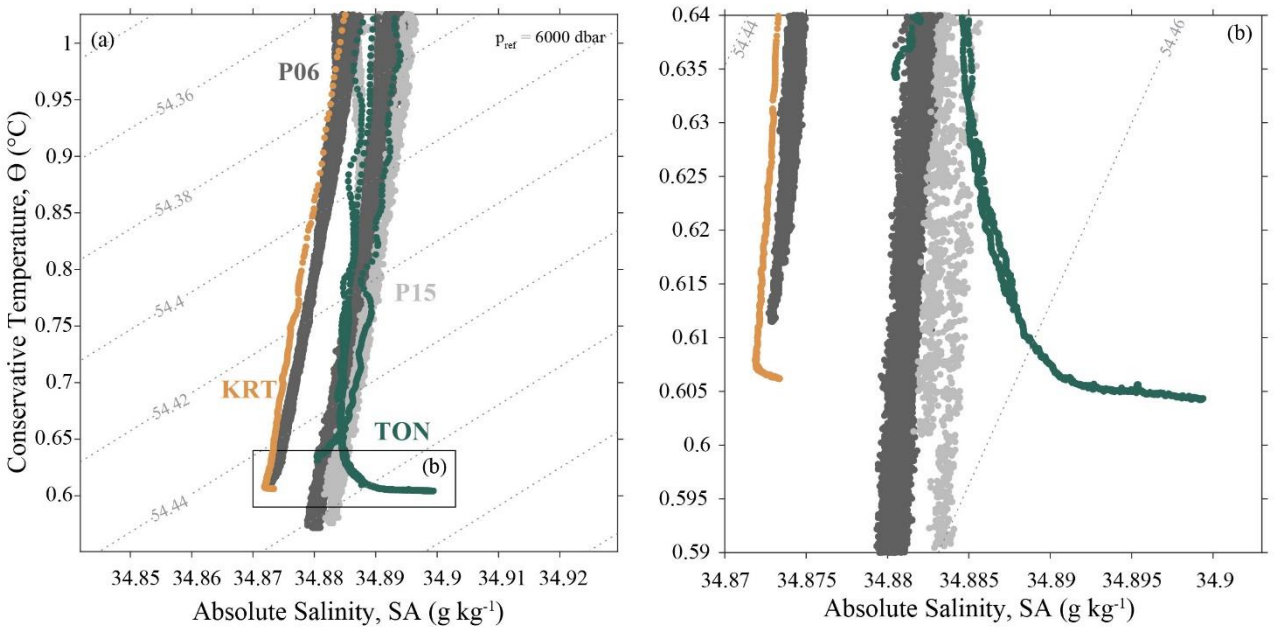

Figure 4. As in Figure 2 for the Kermadec Trench (KRT) and Tonga Trench (TON). The grey is WOCE section P06 and P15.

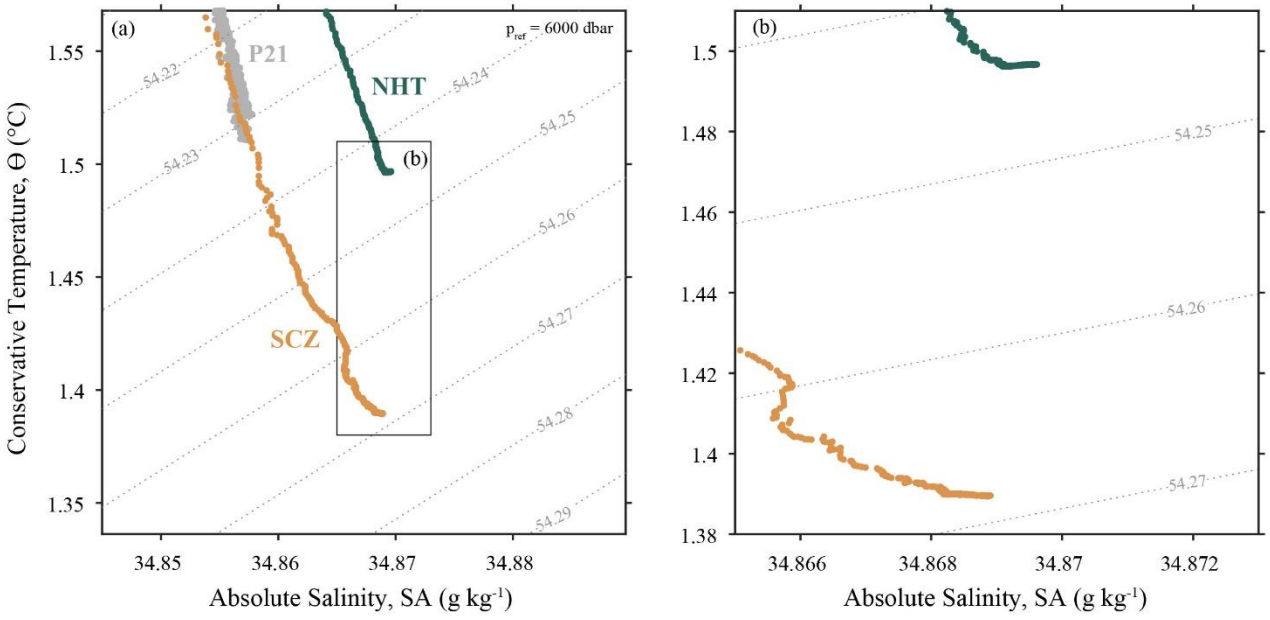

Figure 5. As in Figure 2 for the Santa Cruz Trench (SCZ) and New Hebrides Trench (NHT). The grey is WOCE section P21.

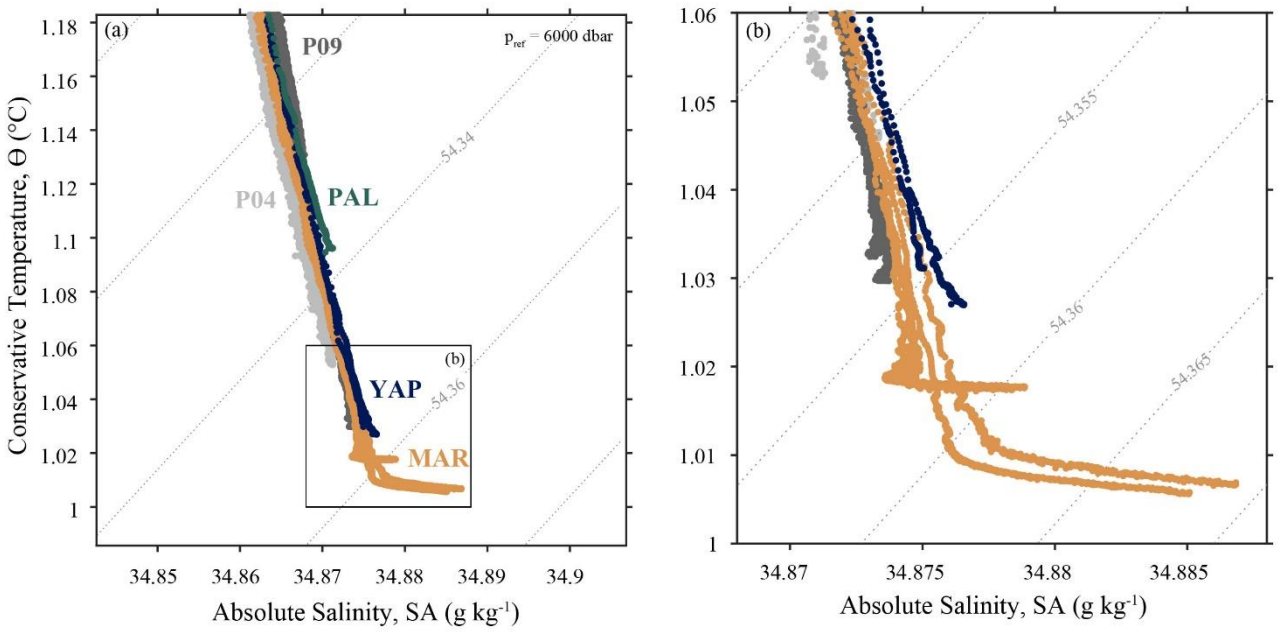

Figure 6. As in Figure 2 for the Mariana Trench (MAR), the Palau Trench (PAL) and Yap Trench (YAP). The grey is WOCE section P04 and P09.

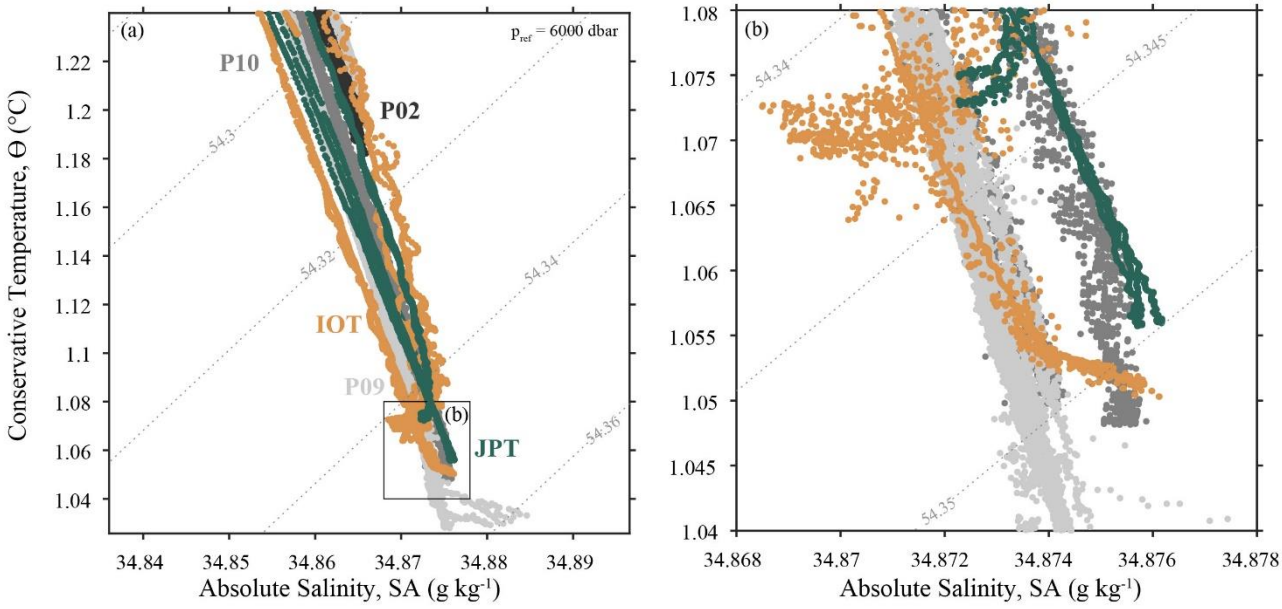

Figure 7. As in Figure 2 for the Japan Trench (JPT) and Izu-Ogasawara Trench (IOT). The grey is WOCE section P09 and P10. N.B the fresh tail increases in GO-SHIP P10 are statistically unstable but within the ±0.002 instrument uncertainty. The same applies to shallow JPT profiles, but not shallower IOT profiles. These IOT profiles were excluded from further analysis.

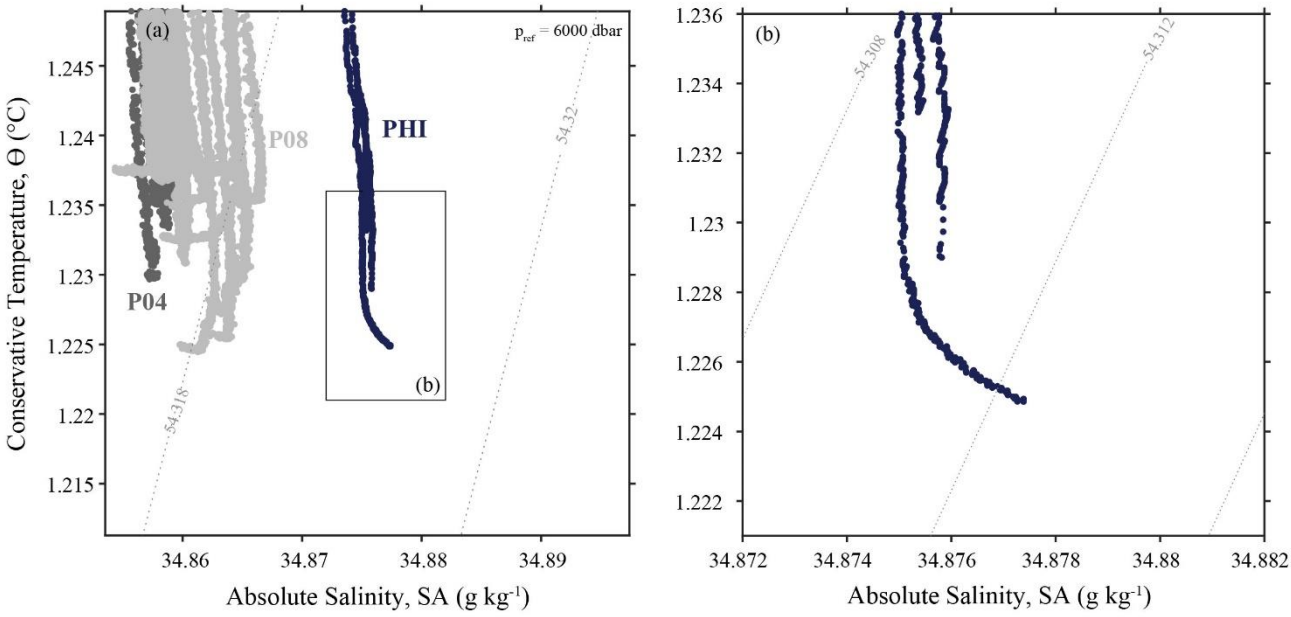

Figure 8. As in Figure 2 for the Philippine Trench. The grey is WOCE section P08 and GO-SHIP P04. N.B the fresh tail increase in P08 is statistically unstable.

3.2 Bottom Conditions

The South Sandwich Trench (SAND) is unique in its location in the Southern Ocean and proximity to bottom water formation compared to the other trenches. It is the coolest (Θ = 0.69ºC, In-situ Temperature, T = 0.03ºC) and most fresh (SA = 34.82 g kg^{-1}) of the trenches observed (Figures 9 and 10). The Java Trench (JAV) is the only observation within the Indian Ocean and is the most saline of the twelve trenches at 7000 dbar (S_A = 34.89 g kg^{-1}) (Figure 9c). The trenches become warmer from south to north along the western Pacific (Figures 9a and c). This excludes NHT and SCZ within the Bougainville-New Hebrides hadal province, which exhibited warmer and fresher water properties than TON-KRT to the east and MAR-YAP-PAL to the north. Within the northwest Pacific, the Philippine Trench (PHI) is the warmest of the trenches surrounding the Philippine Basin in terms of bottom temperature (Θ = 1.24ºC) (Figure 10). The average bottom conditions of the trenches within the same hadal province are within the same Θ-S_A space, with the Mariana and Aleutian-Japan hadal provinces overlapping (Figure 10). These results suggest an association between the bottom conditions in trenches within the same hadal province and their location along the bottom limb of the overturning circulation.

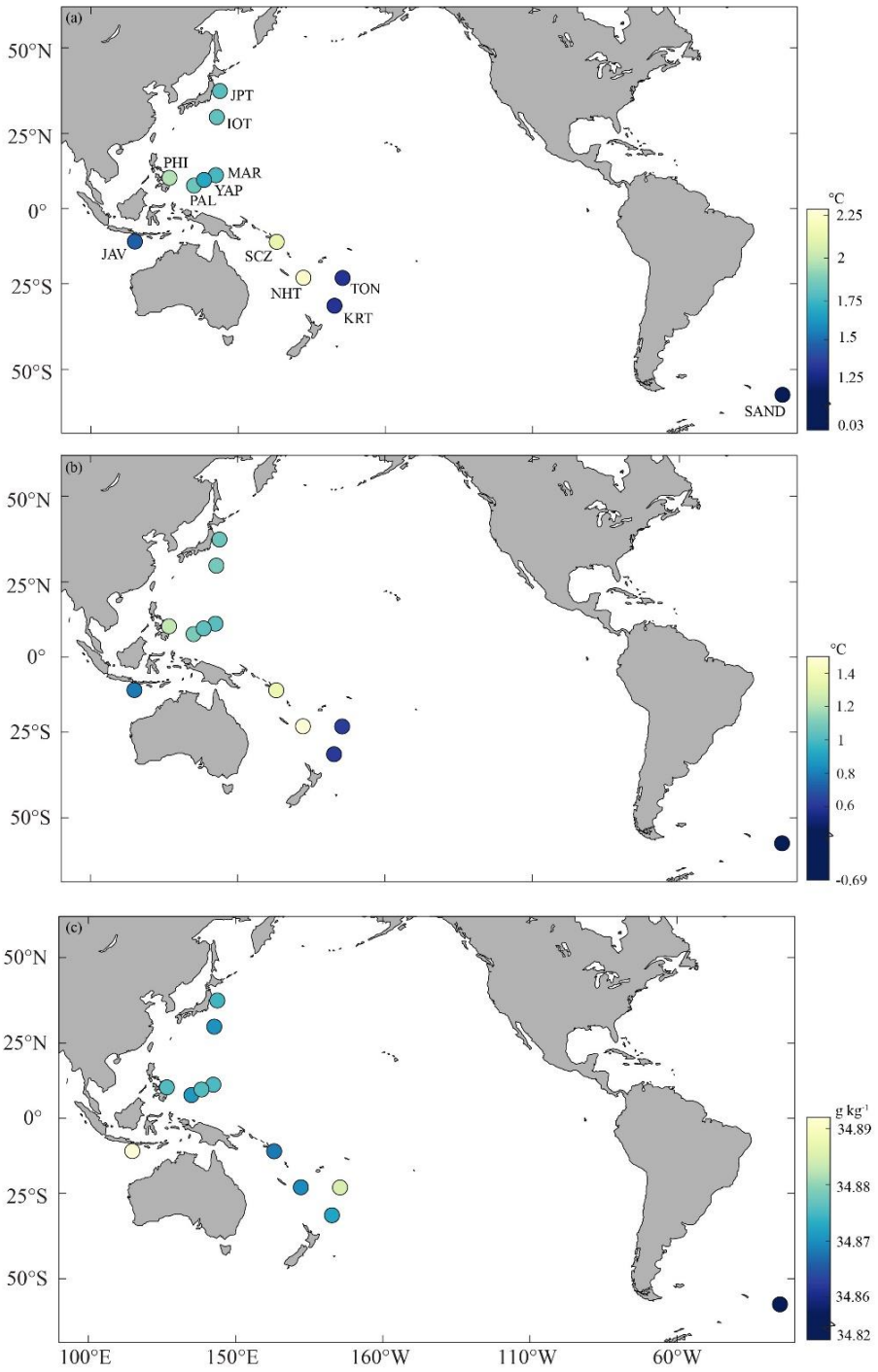

305

Figure 9. Conditions in each trench at 7000 m depth of (a) In-situ Temperature (°C) (b) Conservative Temperature (°C) and (c) Absolute Salinity (g kg-1). JPT, Japan Trench, IOT, Izu-Ogasawara Trench, PHI, Philippine Trench, PAL, Palau Trench, YAP, Yap Trench, MAR, Mariana Trench, SCZ, Santa Cruz Trench, NHT, New Hebrides Trench, KRT, Kermadec Trench, TON, Tonga Trench, JAV, Java Trench, SAND, South Sandwich Trench.

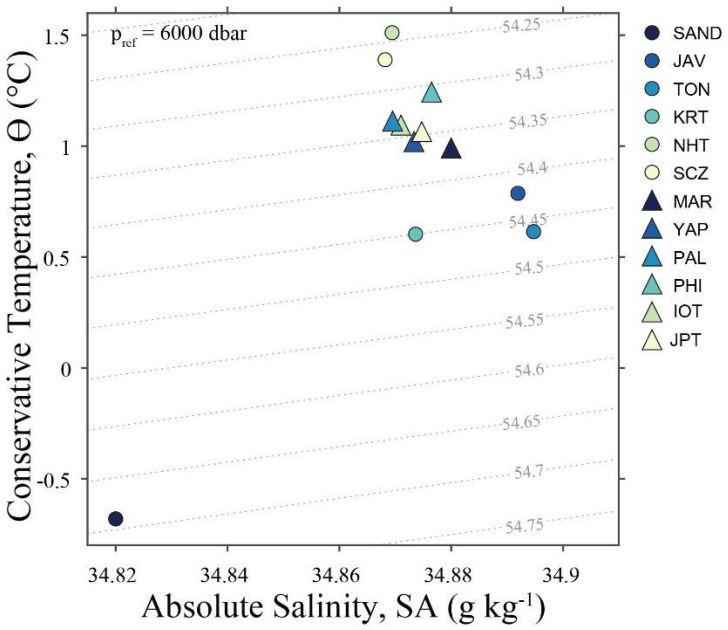

310

Figure 10. Average bottom conditions in Θ-S_A for each trench. Isopycnals (contour lines) show the potential density referenced to 6000 dbar. See Figure 9 for location abbreviations and Table 1 for bottom depth.

3.3 Source water type analysis

Preliminary results indicated vertical variation in the water-mass fractions over the abyssal waters (4000 – 6000 m) and
315 negligible vertical variation in the hadopelagic. Within abyssal waters, the KRT, the southernmost trench of the Pacific, exhibits the greatest proportion of AABW over depth (~0.49) (Figure 11a). The proportion is lower at 4000m for TON (~0.47) (Figure 11b); however, it has a comparable proportion of AABW to KRT throughout the hadopelagic (0.58) (Figure 12). MAR and YAP showed a similar proportion of AABW in abyssal waters (~0.19); however, MAR had a higher proportion of AABW in the hadopelagic (~0.22). The conditions in PAL provided a similar output of AABW proportions to IOT and JPT in both
320 depth ranges. The proportion of AABW in the abyssal waters (~0.03) and the hadopelagic (0.05) were the lowest for PHI. There was a greater range uncertainty due to the source water types (Table 2) in the northern hemisphere than in the southern hemisphere. The range uncertainty is highest for PHI in the abyssal waters (Figure 11f) and the hadopelagic (Figure 12). The more considerable variation in LCDW source water types, compared to AABW (Table 2), had a greater impact on the range uncertainty overall in the northern hemisphere compared to the southern hemisphere. Generally, the proportion of AABW
325 decreases as the distance from the source latitude (60ºS) increases, apart from PHI which exhibits conditions more similar to those of LCDW.

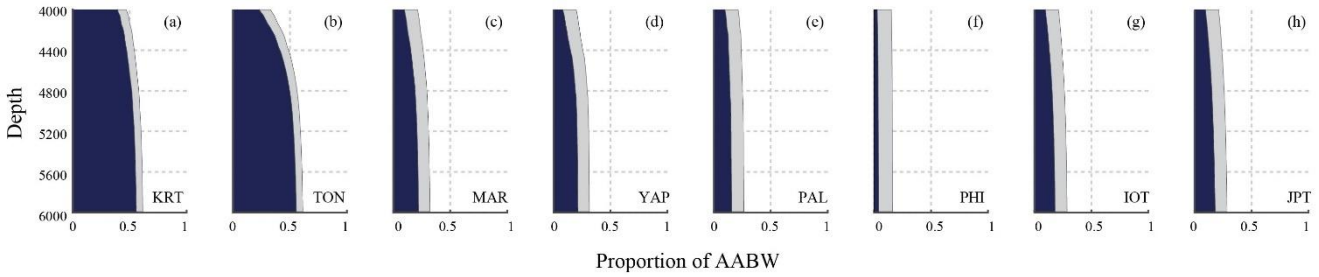

Figure 11. Proportion of Antarctic Bottom Water (AABW) in the abyssal waters above (a) KRT, (b) TON, (c) MAR, (d) €, (e) PAL, (f) PHI, (g) IOT and (h) JPT in the blue shaded profile. The proportion of LCDW is 1 minus the proportion shown. The grey area represents the range uncertainty between possible source water type combinations of AABW and LCDW in the SWT analysis. The standard error of the mean was less than 10^{-4} in all instances.

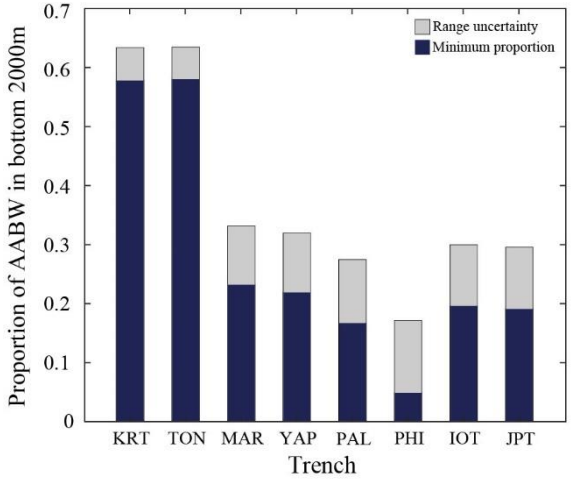

Figure 12. Proportion of AABW in the bottom 2000 m of trenches in the western Pacific. The proportion of LCDW is the remainder of the proportion to equal 1. The range uncertainty is the mean range between possible source water type combinations of AABW and LCDW in the SWT analysis (Table 2). The standard error of the mean was less than 10^{-4} in all instances.

3 Discussion

The variations in trench conditions were consistent within their hadal provinces and current knowledge surrounding bottom water circulation out of the Southern Ocean (Gordon et al., 2020; Naveira Garabato et al., 2002; Talley, 2013a), in the Indian Ocean (Wijffels et al., 2002; Wang et al., 2012; Mantyla and Reid, 1995) and throughout the western Pacific (Liu, 2022; Germineaud et al., 2021; Tian et al., 2021; Zhai and Gu, 2020).

At 7,000 m, the temperature is relatively consistent within the hadal provinces. Consistent differences are seen in T and Θ (Figure 9 a and b). These differences occur between either side of the South Fiji Basin, with TON and KRT being ~1°C cooler than NHT, SCB or SCZ at 6000 m. Surrounding the Philippine Sea, PHI on the eastern side is ~0.2°C warmer than MAR, YAP, and PAL to the southeast and IOT and JPT to the northeast. These two differences in the south and northeast Pacific are likely due to the moving of cold Antarctic Bottom Water (AABW)/Lower Circumpolar Deep Water (LCDW) northward at

hadal depths along the Tonga-Kermadec Ridge and north-eastward to reach Mariana-Yap Junction (Kawabe and Fujio, 2010). The LCDW does not penetrate into the south Philippine Basin due to the Central Basin Fault (Tian et al., 2021), which may explain these differences and the SWT analysis results. The same applies to NHT and SCZ, which are less ventilated by the LCDW (Germineaud et al., 2021).

Our observations revealed fine-scale variations in the hydrographic profiles that require further exploration. The Java Trench, for which we believe is the first full-depth hydrographic profile, displays a Θ-S_A profile shape similar to Bayhaqi et al. (2018) and Atmadipoera et al. (2009). There is a split in the Θ-S_A shape at 0.8°C (Figure 3b), likely due to the opposing movement of bottom water on either side of the trench sills, with the northernmost profile displaying a slightly higher salinity (Zhai and Gu, 2020; Johnson, 1998). A similar diversion appears in the Yap Trench (Figure 6b), with the deeper, saltier profiler nearer to the Yap-Mariana Junction, possibly due to local water isolation at hadal or bottom water depths, as suggested by Liu et al. (2022). Although the CTD profiles for IOT are more variable than neighbouring JPT profiles, they meet our quality control criteria. The IOT profiles display an increase in S_A over a constant Θ of 1.06°C, like the profiles from section P09. The IOT's location within the primary flow path of AABW/LCDW and UCDW may contribute to increased mixing (Zhou et al., 2022; Taira, 2006). Conversely, our observations at PHI show a discrepancy in S_A to the WOCE deployments (Figure 8a), which could be due to temporal differences, conductivity measurement inconsistencies, or possible sensor drift (van Haren et al., 2021; van Haren, 2022; Gouretski et al., 2022). Further supporting this, moored profiles from (Wang et al., 2017), 4° south of our observation shows a lower average S_A (Wang et al., 2017). Given these complexities, additional measurements within these trenches are necessary.

The warmer waters of PHI, and the resulting lowest fraction of AABW in the hadopelagic (0.05±0.01) compared to nearby trenches is consistent with the observed circulation within the Philippine Basin (Tian et al., 2021; Zhai and Gu, 2020; Wang et al., 2017). The bottom water enters through the Yap-Mariana junction, spilling into the Philippine Sea, flowing northward and westward, but blocked to the south by the Central Basin Fault (Tian et al., 2021). Aside from PHI, the proportion of AABW within a trench decreases with increasing distance from the Southern Ocean (Figure 12). Overall, the proportion of AABW within trenches along the western Pacific is consistent with bottom water circulation in the Pacific (Kawabe et al., 2003; Kawabe, 1993). However, our water mass analysis results limited by the constraints placed on the water mass seawater properties used in the analysis. A robust understanding of circulation deeper than 6000 m is rare and biased towards MAR (van Haren et al., 2017; Jiang et al., 2021), while circulation of abyssal waters above the trenches in the Pacific are well described (Liu, 2022; Taft et al., 1991; Kawabe, 1993; Zilberman et al., 2020). Recent studies on PHI describe a cyclonic motion over the southern portion of the trench (Tian et al., 2021; Zhai and Gu, 2020; Wang et al., 2017), originally detailed by Johnson (1998) and present over other trenches (Mitsuzawa and Holloway, 1998; Warren and Brechner Owens, 1985; Huang et al., 2018; Nagano et al., 2013; Ma et al., 2021). Given the difficulties in deploying moored current profilers to hadal depths, where future deployments are limited to CTDs, deployments should be along transects in a meridional or zonal direction to allow calculations of geostrophic velocities within and above the trench sills. Furthermore, deploying sensors with higher

frequency measurements than those included here is needed to uncover details on turbulent mixing processes, geothermal heating considerations and internal wave characteristics within weakly stratified trenches (van Haren, 2020a, 2023; Joyce et al., 1986).

From around 9000 dbar, increases in S_A of approximately 0.003 g kg^{-1}/1000dbar were observed in the KRT, TON, MAR, and PHI trenches, giving "salty-tails". This was despite applying a linear pressure correction to the conductivity data during processing. Similar findings were noted by van Haren et al. (2021) and Taira (2005) in the Mariana Trench. Following discussions with the CTD instrument manufacturer, SeaBird Electronics, we decided against implementing the corrections suggested by van Haren et al. (2021) for a comparable SBE 911 CTD (Seabird pers comms. 2022). The decision was because corrected salinity data still exhibited an increase when the correction was applied. Van Haren et al. (2021) proposed that this increase could signify dense modified AABW mixing with higher salinity LCDW in the trenches over long time scales. This observation is particularly relevant within KRT and TON, which serve as a conduit between LCDW and cold AABW from the south to the north of the Pacific (Reid, 1997; Zilberman et al., 2020). It is likely that the salty tails are due to sensor-dependent interaction between the glass conductivity cells and their protective jacket in the instrument (Kobayashi et al., 2021) which is taken into consideration when correcting for conductivity cell compressibility, however could be different for each instrument. This would explain the differences between the varying rates of S_A increase. Potential real causes include small-scale influences from diapycnal mixing and internal tides (van Haren, 2020a), or saline pore water being expelled from deep-sea sediments due to intense pressures (Oguri et al., 2022; Glud et al., 2013; Turnewitsch et al., 2014), which could result in the salty tails. Without water samples from the trench sill to the trench floor, we cannot confidently confirm or deny the reality of the salty tails. Additionally, GO-SHIP data is limited to 6000 dbar. Nevertheless, in our circumstance, the largest increase in S_A is 0.015 g kg^{-1} over the bottom 1000m of TON compared to the smallest difference in AABW and LCDW S_A of 0.0218 g kg^{-1} (Table 1). Therefore, this slight S_A increase does not significantly affect the water mass proportion over hadal depths in these trenches.

The observed latitude-dependent pattern is key to understanding climate change scenarios, especially alterations in AABW ranging from export rate to warming (Zhou et al., 2023; Jacobs et al., 2022; Bai et al., 2022; Boeira Dias et al., 2023). Warming has been predominant in the Indian Ocean, with contrasting freshening in the eastern region and increased salinity in the western region (Choi and Nam, 2022; Thomas et al., 2020). Similar trends of warming and freshening are well-documented in the Pacific (Purkey et al., 2019; Johnson et al., 2019; Lele et al., 2021) and the Atlantic (Campos et al., 2021; Liu and Tanhua, 2021). Compared to the 1990 WOCE S4, the South Sandwich trench profiles are fresher and warmer, a predictable discrepancy considering the time difference (Gordon et al., 2020; Zhang and Delworth, 2016). We intentionally did not address temporal changes in the WOCE/GO-SHIP sections, given their comprehensive coverage elsewhere (Hautala and Finucane, 2022; Wijffels et al., 2002; Naveira Garabato et al., 2014; Wijffels et al., 1998; Talley, 2013a). While single observations from some trenches provide a preliminary perspective, they should be interpreted cautiously when drawing long-term warming or

freshening trends, even in the overlying abyssal waters (Schmidt et al., 2023). Increased physical data from hadal depths, specifically regions other than the Mariana Trench, are required to thoroughly understand long-term temporal and spatial differences.

Bottom water masses, originating in the high latitudes, ventilate approximately 75% of the ocean below 1,500 m through global overturning circulation (Robinson and Stommel, 1959; Stommel and Arons, 1959; Khatiwala et al., 2012). A trench's conditions over hadal depths are significantly dictated by its geospatial position along the large deep circulation path, introducing complexity and spatial heterogeneity (Kawabe and Fujio, 2010; Kawabe, 1993). Considering these factors, our results are consistent with the current body of knowledge surrounding hadal trenches and add to our understanding. Additionally, trench environments exhibit significant spatial heterogeneity of species, encompassing macrofauna such as amphipods to microscopic life forms, including single-celled organisms and bacteria (Weston et al., 2022; Schauberger et al., 2021; Jing et al., 2018). Intensifying our observational focus and understanding of the physical conditions in the hadopelagic can offer deeper insights into ecological interconnections, diversity, and the driving forces behind such biodiversity. This knowledge is particularly critical considering the vertical transport of organic material into these trenches' sills, a process fundamental for life sustenance (Ichino et al., 2015; Glud et al., 2013). Thus, despite potential enhancements, the baseline environmental conditions elucidated in the current study serve as an indispensable foundation for future research across ecological, biological, or physical oceanographic understanding (Levin et al., 2019).

Conclusion

This study reinforces the importance of understanding hadal trench conditions and their heterogeneity due to their geospatial positions along deep circulation paths. Distinct geographical trends were identified, with the South Sandwich Trench and Java Trench exemplifying diverse profiles due to their respective locations. Vertical variations in water-mass fractions were observed across trenches, with the southernmost Pacific trench, the Kermadec Trench, holding the most substantial Antarctic Bottom Water proportion. Warmer waters in the Philippine Trench indicated reduced Antarctic Bottom Water presence, consistent with its remote location on the western-most side of the Philippine Sea. A consistent salinity increase at depth across several trenches was noted, possibly due to deep-sea sediment processes or water mass mixing. Latitude-dependent patterns are crucial for understanding potential climate change scenarios and suggest consistent warming and freshening trends in the Indian, Pacific, and Atlantic Oceans. The study provides valuable baseline conditions for future ecological, biological, and physical oceanographic exploration and underscores the need for high-frequency sensor deployment and expanded trench coverage.

Code availability

NA

Data availability

Data will be available through PANGEA

Supplement link

Link to supplementary pdf

Author contribution

JK completed the data processing, data analysis and prepared the manuscript. JK and JZ designed the data analysis. AJ collected the data. CP provided data presentation suggestions and edits.

Competing interests

The authors declare that they have no conflict of interest.

Acknowledgements

We thank the captain, crew, and company of the DSSV *Pressure Drop* during the 'Five Deeps' expedition and 'Ring of Fire' expeditions. We thank Victor Vescovo and Cassie Bongiovanni (Caladan Oceanic LLC, US), Patrick Lahey, Shane Eigler, Tim Macdonald (Triton Submarines LLC, US), Rob McCallum (EYOS Expeditions, UK). The authors would also like to thank Devin Harrison for the map in the Supplementary information that was made for this publication.

References

Abernathey, R. P., Cerovecki, I., Holland, P. R., Newsom, E., Mazloff, M., and Talley, L. D.: Water-mass transformation by sea ice in the upper branch of the Southern Ocean overturning, Nat. Geosci., 9, 596–601, https://doi.org/10.1038/ngeo2749, 2016.

Arvapalli., S. R., Bajish, C. C., and Kurian P, J.: Hydrographic observations in the rift valley of Southwest Indian Ridge from 63°E – 69°E, Dyn. Atmospheres Oceans, 97, 101284, https://doi.org/10.1016/j.dynatmoce.2022.101284, 2022.

Atmadipoera, A., Molcard, R., Madec, G., Wijffels, S. E., Sprintall, J., Koch-Larrouy, A., Jaya, I., and Supangat, A.: Characteristics and variability of the Indonesian throughflow water at the outflow straits, Deep Sea Res. Part Oceanogr. Res. Pap., 56, 1942–1954, https://doi.org/10.1016/j.dsr.2009.06.004, 2009.

Bai, Y., Zhao, L., Xiao, J., and Lin, S.: Contraction and warming of Antarctic Bottom Water in the Amundsen Sea, Acta Oceanol. Sin., 41, 68–79, https://doi.org/10.1007/s13131-021-1829-8, 2022.

Bayhaqi, A., Iskandar, I., Surinati, D., Budiman, A. S., Wardhana, A. K., Dirhamsyah, Yuan, D., and Lestari, D. O.: Water mass characteristic in the outflow region of the Indonesian throughflow during and post 2016 negative Indian ocean dipole event, IOP Conf. Ser. Earth Environ. Sci., 149, https://doi.org/10.1088/1755-1315/149/1/012053, 2018.

Belyaev, G. M.: Deep-Sea Ocean Trenches and Their Fauna, Nauka, Moscow, 1989.

Boeira Dias, F., Rintoul, S. R., Richter, O., Galton-Fenzi, B. K., Zika, J. D., Pellichero, V., and Uotila, P.: Sensitivity of simulated water mass transformation on the Antarctic shelf to tides, topography and model resolution, Front. Mar. Sci., 10, 2023.

Bongiovanni, C., Stewart, H. A., and Jamieson, A. J.: High-resolution multibeam sonar bathymetry of the deepest place in each ocean, Geosci. Data J., https://doi.org/10.1002/gdj3.122, 2021.

Campos, E. J. D., van Caspel, M. C., Zenk, W., Morozov, E. G., Frey, D. I., Piola, A. R., Meinen, C. S., Sato, O. T., Perez, R. C., and Dong, S.: Warming Trend in Antarctic Bottom Water in the Vema Channel in the South Atlantic, Geophys. Res. Lett., 48, https://doi.org/10.1029/2021GL094709, 2021.

Chinni, V., Singh, S., Bhushan, R., Rengarajan, R., and Sarma, V.: Spatial variability in dissolved iron concentrations in the marginal and open waters of the Indian Ocean, Mar. Chem., 208, 11–28, https://doi.org/10.1016/j.marchem.2018.11.007, 2019.

Choi, Y. and Nam, S.: East–west contrasting changes in Southern Indian Ocean Antarctic Bottom Water salinity over three decades, Sci. Rep., 12, 12175, https://doi.org/10.1038/s41598-022-16331-y, 2022.

Cimoli, L., Mashayek, A., Johnson, H. L., Marshall, D. P., Naveira Garabato, A. C., Whalen, C. B., Vic, C., de Lavergne, C., Alford, M. H., MacKinnon, J. A., and Talley, L. D.: Significance of Diapycnal Mixing Within the Atlantic Meridional Overturning Circulation, AGU Adv., 4, e2022AV000800, https://doi.org/10.1029/2022AV000800, 2023.

Dickson, R. R. and Brown, J.: The production of North Atlantic Deep Water: sources, rates, and pathways, J. Geophys. Res., 99, 12 319-12 341, https://doi.org/10.1029/94jc00530, 1994.

Fine, R. A., Smethie, W. M., Bullister, J. L., Rhein, M., Min, D.-H., Warner, M. J., Poisson, A., and Weiss, R. F.: Decadal ventilation and mixing of Indian Ocean waters, Deep Sea Res. Part Oceanogr. Res. Pap., 55, 20–37, https://doi.org/10.1016/j.dsr.2007.10.002, 2008.

Fujio, S.: Deep current measurements at 38°N east of Japan, J. Geophys. Res., 110, C02010, https://doi.org/10.1029/2004JC002288, 2005.

Fujio, S., Yanagimoto, D., and Taira, K.: Deep current structure above the Izu-Ogasawara Trench, J. Geophys. Res., 105, 6377–6386, 2000.

Ganachaud, A.: Large-scale mass transports, water mass formation, and diffusivities estimated from World Ocean Circulation Experiment (WOCE) hydrographic data, J. Geophys. Res., 108, 3213, https://doi.org/10.1029/2002JC001565, 2003.

Ganachaud, A. and Wunsch, C.: Improved estimates of global ocean circulation, heat transport and mixing from hydrographic data, Nature, 408, 453–457, 2000.

Germineaud, C., Cravatte, S., Sprintall, J., Alberty, M., Grenier, M., and Ganachaud, A.: Deep pacific circulation: New insights on pathways through the Solomon Sea, Deep Sea Res. Part Oceanogr. Res. Pap., 171, 103510, https://doi.org/10.1016/j.dsr.2021.103510, 2021.

Glud, R. N., Wenzhöfer, F., Middelboe, M., Oguri, K., Turnewitsch, R., Canfield, D. E., and Kitazato, H.: High rates of microbial carbon turnover in sediments in the deepest oceanic trench on Earth, Nat. Geosci., 6, 284–288, https://doi.org/10.1038/ngeo1773, 2013.

Goodman, P. J.: The Role of North Atlantic Deep Water Formation in an OGCM's Ventilation and Thermohaline Circulation, J. Phys. Oceanogr., 28, 1759–1785, https://doi.org/10.1175/1520-0485(1998)028<1759:TRONAD>2.0.CO;2, 1998.

Gordon, A. L.: Interocean exchange of thermocline water, J. Geophys. Res. Oceans, 91, 5037–5046, https://doi.org/10.1029/JC091iC04p05037, 1986a.

Gordon, A. L.: Is there a global scale ocean circulation?, Eos Trans. Am. Geophys. Union, 67, 109–110, https://doi.org/10.1029/EO067i009p00109, 1986b.

Gordon, A. L., Huber, B. A., and Abrahamsen, E. P.: Interannual Variability of the Outflow of Weddell Sea Bottom Water, Geophys. Res. Lett., 47, https://doi.org/10.1029/2020GL087014, 2020.

Gouretski, V., Cheng, L., and Boyer, T.: On the Consistency of the Bottle and CTD Profile Data, J. Atmospheric Ocean. Technol., 39, 1869–1887, https://doi.org/10.1175/JTECH-D-22-0004.1, 2022.

Greenaway, S. F., Sullivan, K. D., Umfress, H., Beittel, A. B., and Wagner, K. D.: Revised depth of the Challenger Deep from submersible transects; including a general method for precise, pressure-derived depths in the ocean, Deep-Sea Res. Part Oceanogr. Res. Pap., 178, https://doi.org/10.1016/j.dsr.2021.103644, 2021.

van Haren, H.: Challenger Deep internal wave turbulence events, Deep-Sea Res. Part Oceanogr. Res. Pap., 165, https://doi.org/10.1016/j.dsr.2020.103400, 2020a.

van Haren, H.: Slow persistent mixing in the abyss, Ocean Dyn., 70, 339–352, 2020b.

van Haren, H.: Thermistor string corrections in data from very weakly stratified deep-ocean waters, Deep-Sea Res. Part Oceanogr. Res. Pap., 189, https://doi.org/10.1016/j.dsr.2022.103870, 2022.

van Haren, H.: How and what turbulent are deep Mariana Trench waters?, Dyn. Atmospheres Oceans, 103, 101372, https://doi.org/10.1016/j.dynatmoce.2023.101372, 2023.

van Haren, H., Berndt, C., and Klaucke, I.: Ocean mixing in deep-sea trenches: New insights from the Challenger Deep, Mariana Trench, Deep-Sea Res. Part Oceanogr. Res. Pap., 129, 1–9, https://doi.org/10.1016/j.dsr.2017.09.003, 2017.

van Haren, H., Uchida, H., and Yanagimoto, D.: Further correcting pressure effects on SBE911 CTD-conductivity data from hadal depths, J. Oceanogr., 77, 137–144, https://doi.org/10.1007/s10872-020-00565-3, 2021.

Hautala, S. L. and Finucane, G.: Persistence of the Large-Scale Interior Deep Ocean Circulation in Global Repeat Hydrographic Sections, Geophys. Res. Lett., 49, https://doi.org/10.1029/2021GL097264, 2022.

Helland-Hansen, B.: Nogen hydrografiske metoder, Naturforsker Möte Kristiania, 1916.

Huang, C., Xie, Q., Wang, D., Shu, Y., Xu, H., Xiao, J., Zu, T., Long, T., and Zhang, T.: Seasonal variability of water characteristics in the Challenger Deep observed by four cruises, Sci. Rep., 8, https://doi.org/10.1038/s41598-018-30176-4, 2018.

Ichino, M. C., Clark, M. R., Drazen, J. C., Jamieson, A. J., Jones, D. O. B., Martin, A. P., Rowden, A. A., Shank, T. M., Yancey, P. H., and Ruhl, H. A.: The distribution of benthic biomass in hadal trenches: A modelling approach to investigate the effect of vertical and lateral organic matter transport to the seafloor, Deep Sea Res. Part Oceanogr. Res. Pap., 100, 21–33, https://doi.org/10.1016/j.dsr.2015.01.010, 2015.

IOC, SCOR, and IAPSO: The international thermodynamic equation of seawater - 2010: Calculations and use of thermodynmic properties, 2010.

Jacobs, S. S., Giulivi, C. F., and Dutrieux, P.: Persistent Ross Sea Freshening From Imbalance West Antarctic Ice Shelf Melting, J. Geophys. Res. Oceans, 127, https://doi.org/10.1029/2021JC017808, 2022.

Jamieson, A. and Linley, T.: Hydrozoans, scyphozoans, larvaceans and ctenophores observed in situ at hadal depths, J. Plankton Res., 43, 20–32, https://doi.org/10.1093/plankt/fbaa062, 2021.

Jamieson, A. J.: The Hadal Zone; Life in the Deepest Oceans, Cambridge University Press, 2015.

Jamieson, A. J.: A contemporary perspective on hadal science, Deep-Sea Res. Part II Top. Stud. Oceanogr., 155, 4–10, https://doi.org/10.1016/j.dsr2.2018.01.005, 2018.

Jamieson, A. J. and Fujii, T.: Trench Connection, Biol. Lett., 7, 641–643, https://doi.org/10.1098/rsbl.2011.0231, 2011.

Jamieson, A. J. and Stewart, H. A.: Hadal zones of the Northwest Pacific Ocean, Prog. Oceanogr., 190, https://doi.org/10.1016/j.pocean.2020.102477, 2021.

Jamieson, A. J., Fujii, T., Mayor, D. J., Solan, M., and Priede, I. G.: Hadal trenches: the ecology of the deepest places on Earth, Trends Ecol. Evol., 25, 190–197, https://doi.org/10.1016/j.tree.2009.09.009, 2010.

Jamieson, A. J., Stewart, H. A., Rowden, A. A., and Clark, M. R.: Geomorphology and benthic habitats of the Kermadec Trench, Southwest Pacific Ocean, in: Seafloor Geomorphology as Benthic Habitat, Elsevier, 949–966, 2020.

Jamieson, A. J., Linley, T. D., Eigler, S., and Macdonald, T.: A global assessment of fishes at lower abyssal and upper hadal depths (5000 to 8000 m), Deep Sea Res. Part Oceanogr. Res. Pap., 178, 103642, 2021a.

Jamieson, A. J., Stewart, H. A., Weston, J., and Bongiovanni, C.: Hadal fauna of the South Sandwich Trench, Southern Ocean: Baited camera survey from the Five Deeps Expedition., Deep-Sea Res. Part II Top. Stud. Oceanogr., 194, https://doi.org/10.1016/j.dsr2.2021.104987, 2021b.

Jamieson, A. J., Bond, T., and Vescovo, V.: No recovery of a large-scale anthropogenic sediment disturbance on the Pacific seafloor after 77 years at 6460 m depth, Mar. Pollut. Bull., 175, 113374–113374, https://doi.org/10.1016/j.marpolbul.2022.113374, 2022.

Jiang, H., Xu, H., Vetter, P. A., Xie, Q., Yu, J., Shang, X., and Yu, L.: Ocean Circulation in the Challenger Deep Derived From Super-Deep Underwater Glider Observation, Geophys. Res. Lett., 48, e2021GL093169, 2021.

Johnson, G. C.: Deep water properties, velocities, and dynamics over ocean trenches, J. Mar. Res., 56, 329–347, https://doi.org/10.1357/002224098321822339, 1998.

Johnson, G. C.: Quantifying Antarctic Bottom Water and North Atlantic Deep Water volumes, J. Geophys. Res. Oceans, 113, 1–13, https://doi.org/10.1029/2007JC004477, 2008.

Johnson, G. C., Purkey, S. G., Zilberman, N. V., and Roemmich, D.: Deep Argo quantifies bottom water warming rates in the Southwest Pacific Basin, Geophys. Res. Lett., 46, 2662–2669, 2019.

Joyce, T. M., Warren, B. A., and Talley, L. D.: The geothermal heating of the abyssal subarctic Pacific Ocean, Deep Sea Res. Part Oceanogr. Res. Pap., 33, 1003–1015, https://doi.org/10.1016/0198-0149(86)90026-9, 1986.

Karstensen, J. and Tomczak, M.: Age determination of mixed water masses using CFC and oxygen data, J. Geophys. Res. Oceans, 103, 18599–18609, https://doi.org/10.1029/98JC00889, 1998.

Katsumata, K. and Fukasawa, M.: Changes in meridional fluxes and water properties in the Southern Hemisphere subtropical oceans between 1992/1995 and 2003/2004, Prog. Oceanogr., 89, 61–91, https://doi.org/10.1016/j.pocean.2010.12.008, 2011.

Kawabe, M.: Deep Water Properties and Circulation in the Western North Pacific, in: Deep Ocean Circulation, Physical and Chemical Aspects, edited by: Teramoto, T., Elsevier, Amsterdam, 17–37, 1993.

Kawabe, M. and Fujio, S.: Pacific ocean Circulation Based on Observation, J. Oceanogr., 66, 389–403, https://doi.org/10.1007/s10872-010-0034-8, 2010.

Kawabe, M., Fujio, S., and Yanagimoto, D.: Deep-water circulation at low latitudes in the western North Pacific, Deep-Sea Res. Part Oceanogr. Res. Pap., 50, 631–656, https://doi.org/10.1016/S0967-0637(03)00040-2, 2003.

Kawagucci, S., Makabe, A., Kodama, T., Matsui, Y., Yoshikawa, C., Ono, E., Wakita, M., Nunoura, T., Uchida, H., and Yokokawa, T.: Hadal water biogeochemistry over the Izu-Ogasawara Trench observed with a full-depth CTD-CMS, Ocean Sci., 14, 575–588, https://doi.org/10.5194/os-14-575-2018, 2018.

Khatiwala, S., Primeau, F., and Holzer, M.: Ventilation of the deep ocean constrained with tracer observations and implications for radiocarbon estimates of ideal mean age, Earth Planet. Sci. Lett., 325–326, 116–125, https://doi.org/10.1016/j.epsl.2012.01.038, 2012.

Kobayashi, T., Sato, K., and King, B. A.: Observed features of salinity bias with negative pressure dependency for measurements by SBE 41CP and SBE 61 CTD sensors on deep profiling floats, Prog. Oceanogr., 198, 102686, https://doi.org/10.1016/j.pocean.2021.102686, 2021.

Koltermann, K. P., Gouretski, V., and Jancke, K.: Hydrographic Atlas of the World Ocean Circulation Experiment (WOCE): Volume 3: Atlantic Ocean, 2011.

Leffanue, H. and Tomczak, M.: Using OMP analysis to observe temporal variability in water mass distribution, J. Mar. Syst., 48, 3–14, https://doi.org/10.1016/j.jmarsys.2003.07.004, 2004.

Lele, R., Purkey, S. G., Nash, J. D., Mackinnon, J. A., Thurnherr, A. M., Whalen, C. B., Mecking, S., Voet, G., and Talley, L. D.: Abyssal Heat Budget in the Southwest Pacific Basin, J. Phys. Oceanogr., 51, 3317–3333, https://doi.org/10.1175/JPO-D-21-0045.1, 2021.

Liu, M. and Tanhua, T.: Water masses in the Atlantic Ocean: characteristics and distributions, Ocean Sci., 17, 463–486, https://doi.org/10.5194/os-17-463-2021, 2021.

Liu, X.: Flow Pathways of Abyssal Water in the Yap Trench and Adjacent Channels and Basins, Front. Mar. Sci., 9, 16, 2022.

Liu, X., Liu, Y., Cao, W., and Sun, C.: Water characteristics of abyssal and hadal zones in the southern Yap Trench observed with the submersible Jiaolong, J. Oceanol. Limnol., 38, 593–605, https://doi.org/10.1007/s00343-019-8368-6, 2020.

Ma, K., Chen, Z.-H., Li, Z.-R., Song, Z.-J., Yuan, Z.-W., Wu, B., Jiao, Q., and Wang, Z.-M.: Study on 10 000-m Hydrological Observations in the Mariana Trench, Oceanol. Limnol. Sin., 52, 1075–1087, https://doi.org/10.11693/hyhz20201100320, 2021.

Macdonald, A., Mecking, S., Robbins, P., Toole, J., Johnson, G., Talley, L., Cook, M., and Wijffels, S. E.: The WOCE-era 3-D Pacific Ocean circulation and heat budget, https://doi.org/10.1016/J.POCEAN.2009.08.002, 2009.

Mantyla, A. W. and Reid, J. L.: Measurements of water characteristics at depths greater than 10 km in the Marianas Trench, Deep-Sea Res., 25, 169–173, https://doi.org/10.1016/0146-6291(78)90004-8, 1978.

Mantyla, A. W. and Reid, J. L.: On the origins of deep and bottom waters of the Indian Ocean, J. Geophys. Res. Oceans, 100, 2417–2439, 1995.

Mitsuzawa, K. and Holloway, G.: Characteristics of deep currents along trenches in the northwest Pacific, J. Geophys. Res. Oceans, 103, 13085–13092, 1998.

Nagano, A., Ichikawa, K., Ichikawa, H., Yoshikawa, Y., and Murakami, K.: Large ageostrophic currents in the abyssal layer southeast of Kyushu, Japan, by direct measurement of LADCP, J. Oceanogr., 69, 259–268, https://doi.org/10.1007/s10872-013-0170-z, 2013.

Naveira Garabato, A. C., McDonagh, E. L., Stevens, D. P., Heywood, K. J., and Sanders, R. J.: On the export of Antarctic Bottom Water from the Weddell Sea, Deep-Sea Res. Part II Top. Stud. Oceanogr., 49, 4715–4742, https://doi.org/10.1016/S0967-0645(02)00156-X, 2002.

Naveira Garabato, A. C., Williams, A. P., and Bacon, S.: The three-dimensional overturning circulation of the Southern Ocean during the WOCE era, Prog. Oceanogr., 120, 41–78, https://doi.org/10.1016/j.pocean.2013.07.018, 2014.

Naveira Garabato, A. C., MacGilchrist, G. A., Brown, P. J., Evans, D. G., Meijers, A. J., and Zika, J. D.: High-latitude ocean ventilation and its role in Earth's climate transitions, Philos. Trans. R. Soc. Math. Phys. Eng. Sci., 375, 20160324, 2017.

Nunoura, T., Hirai, M., Yoshida-Takashima, Y., Nishizawa, M., Kawagucci, S., Yokokawa, T., Miyazaki, J., Koide, O., Makita, H., Takaki, Y., Sunamura, M., and Takai, K.: Distribution and niche separation of planktonic microbial communities in the water columns from the surface to the hadal waters of the Japan Trench under the Eutrophic Ocean, Front. Microbiol., 7, 1–12, https://doi.org/10.3389/fmicb.2016.01261, 2016.

Oguri, K., Kawamura, K., Sakaguchi, A., Toyofuku, T., Kasaya, T., Murayama, M., Fujikura, K., Glud, R. N., and Kitazato, H.: Hadal disturbance in the Japan Trench induced by the 2011 Tohoku-Oki earthquake, Sci. Rep., 3, https://doi.org/10.1038/srep01915, 2013.

Oguri, K., Masqué, P., Zabel, M., Stewart, H. A., MacKinnon, G., Rowden, A. A., Berg, P., Wenzhöfer, F., and Glud, R. N.: Sediment Accumulation and Carbon Burial in Four Hadal Trench Systems, J. Geophys. Res. Biogeosciences, 127, https://doi.org/10.1029/2022JG006814, 2022.

Orsi, A. H. and Whitworth, T.: Hydrographic Atlas of the World Ocean Circulation Experiment (WOCE): Volume 1: Southern Ocean, WOCE International Project Office Southampton, UK, 2005.

Orsi, A. H., Nowlin, W. D., and Whitworth, T.: On the circulation and stratification of the Weddell Gyre, Deep-Sea Res. Part I, 40, 169–203, https://doi.org/10.1016/0967-0637(93)90060-G, 1993.

Orsi, A. H., Johnson, G. C., and Bullister, J. L.: Circulation, mixing, and production of Antarctic Bottom Water, Prog. Oceanogr., 43, 55–109, https://doi.org/10.1016/S0079-6611(99)00004-X, 1999.

Pond, S. and Pickard, G. L.: Introductory dynamical oceanography, Gulf Professional Publishing, 1983.

Purkey, S. G., Johnson, G. C., Talley, L. D., Sloyan, B. M., Wijffels, S. E., Smethie, W., Mecking, S., and Katsumata, K.: Unabated Bottom Water Warming and Freshening in the South Pacific Ocean, J. Geophys. Res. Oceans, 124, 1778–1794, https://doi.org/10.1029/2018JC014775, 2019.

Rahmstorf, S. and England, M. H.: Influence of Southern Hemisphere Winds on North Atlantic Deep Water Flow, J. Phys. Oceanogr., 27, 2040–2054, https://doi.org/10.1175/1520-0485(1997)027<2040:IOSHWO>2.0.CO;2, 1997.

Rintoul, S. R.: On the Origin and Influence of Adélie Land Bottom Water, in: Ocean, Ice, and Atmosphere: Interactions at the Antarctic Continental Margin, American Geophysical Union (AGU), 151–171, https://doi.org/10.1029/AR075p0151, 1985.

Robinson, A. and Stommel, H.: The oceanic thermocline and the associated thermohaline circulation 1, Tellus, 11, 295–308, 1959.

Roemmich, D., Hautala, S., and Rudnick, D.: Northward abyssal transport through the Samoan passage and adjacent regions, https://doi.org/10.1029/96JC00797, 1996.

Schmidt, C., Morrison, A. K., and England, M. H.: Wind– and sea-ice–driven interannual variability of Antarctic Bottom Water formation, J. Geophys. Res. Oceans, https://doi.org/10.1029/2023JC019774, 2023.

Schmitz, W.: On the interbasin-scale thermohaline circulation, Rev. Geophys., 33, 151–173, 1995.

Sea-Bird Scientific: SBE Data Processing, 2018.

Sea-Bird Scientific: SBE 49 FastCAT CTD Sensor User Manual, Bellevue, Washington, USA, 2020.

Siedler, G., Holfort, J., Zenk, W., Müller, T. J., and Csernok, T.: Deep-water flow in the Mariana and Caroline Basins, J. Phys. Oceanogr., 34, 566–581, https://doi.org/10.1175/2511.1, 2004.

Singh, S. P., Singh, S. K., Goswami, V., Bhushan, R., and Rai, V. K.: Spatial distribution of dissolved neodymium and εNd in the Bay of Bengal: Role of particulate matter and mixing of water masses, Geochim. Cosmochim. Acta, 94, 38–56, https://doi.org/10.1016/j.gca.2012.07.017, 2012.

Sloyan, B. M.: Antarctic bottom and lower circumpolar deep water circulation in the eastern Indian Ocean, J. Geophys. Res. Oceans, 111, https://doi.org/10.1029/2005JC003011, 2006.

Sloyan, B. M. and Rintoul, S. R.: The Southern Ocean Limb of the Global Deep Overturning Circulation, J. Phys. Oceanogr., 31, 143–173, https://doi.org/10.1175/1520-0485(2001)031<0143:TSOLOT>2.0.CO;2, 2001.

Sloyan, B. M., Wanninkhof, R., Kramp, M., Johnson, G. C., Talley, L. D., Tanhua, T., McDonagh, E., Cusack, C., O'Rourke, E., McGovern, E., Katsumata, K., Diggs, S., Hummon, J., Ishii, M., Azetsu-Scott, K., Boss, E., Ansorge, I., Perez, F. F., Mercier, H., Williams, M. J. M., Anderson, L., Lee, J. H., Murata, A., Kouketsu, S., Jeansson, E., Hoppema, M., and Campos, E.: The Global Ocean Ship-Based Hydrographic Investigations Program (GO-SHIP): A Platform for Integrated Multidisciplinary Ocean Science, Front. Mar. Sci., 6, 2019.

Solodoch, A., Stewart, A. L., Hogg, A. McC., Morrison, A. K., Kiss, A. E., Thompson, A. F., Purkey, S. G., and Cimoli, L.: How Does Antarctic Bottom Water Cross the Southern Ocean?, Geophys. Res. Lett., 49, e2021GL097211, https://doi.org/10.1029/2021GL097211, 2022.

Stewart, H. A. and Jamieson, A. J.: Habitat heterogeneity of hadal trenches: Considerations and implications for future studies, Prog. Oceanogr., 161, 47–65, https://doi.org/10.1016/j.pocean.2018.01.007, 2018.

Stommel, H. and Arons, A. B.: On the abyssal circulation of the world ocean-I. Stationary planetary flow patterns on a sphere, Deep-Sea Res., 5, 80–82, 1959.

Swan, J. A., Jamieson, A. J., Linley, T. D., and Yancey, P. H.: Worldwide distribution and depth limits of decapod crustaceans (Penaeoidea, Oplophoroidea) across the abyssal-hadal transition zone of eleven subduction trenches and five additional deep-sea features, J. Crustac. Biol., 41, ruaa102, 2021.

Taft, B. A., Hayes, S. P., Fruederich, G. E., and Codispoti, A.: Flow of Abyssal Water into the Samoa Passage, Deep-Sea Res., 38, 103–128, 1991.

Taira, K.: Super-deep CTD Measurements in the Izu-Ogasawara Trench and a Comparison of Geostrophic Shears with Direct Measurements, J. Oceanogr., 62, 753–758, 2006.

Taira, K., Kitagawa, S., Yamashiro, T., and Yanagimoto, D.: Deep and Bottom Currents in the Challenger Deep, Mariana Trench, Measured with Super-Deep Current Meters, J. Oceanogr., 60, 919–926, 2004.

Taira, K., Yanagimoto, D., and Kitagawa, S.: Deep CTD Casts in the Challenger Deep, Mariana Trench, J. Oceanogr., 61, 447–454, 2005.

Talley, L. D.: Hydrographic Atlas of the World Ocean Circulation Experiment (WOCE) Volume 2: Pacific Ocean, WOCE International Project Office Southampton, 2007.

Talley, L. D.: Descriptive physical oceangraphy: an introduction, Academic Press, 2011.

Talley, L. D.: Closure of the global overturning circulation through the Indian, Pacific, and southern oceans, Oceanography, 26, 80–97, https://doi.org/10.5670/oceanog.2013.07, 2013a.

Talley, L. D.: Hydrographic Atlas of the World Ocean Circulation Experiment (WOCE) Volume 4: Indian Ocean, eScholarship, University of California, 2013b.

Tamsitt, V., Abernathey, R. P., Mazloff, M. R., Wang, J., and Talley, L. D.: Transformation of Deep Water Masses Along Lagrangian Upwelling Pathways in the Southern Ocean, J. Geophys. Res. Oceans, 123, 1994–2017, https://doi.org/10.1002/2017JC013409, 2018.

Thomas, G., Purkey, S. G., Roemmich, D., Foppert, A., and Rintoul, S. R.: Spatial Variability of Antarctic Bottom Water in the Australian Antarctic Basin From 2018–2020 Captured by Deep Argo, Geophys. Res. Lett., 47, https://doi.org/10.1029/2020GL089467, 2020.

Tian, Z., Zhou, C., Xiao, X., Wang, T., Qu, T., Yang, Q., Zhao, W., and Tian, J.: Water-Mass Properties and Circulation in the Deep and Abyssal Philippine Sea, J. Geophys. Res. Oceans, 126, https://doi.org/10.1029/2020JC016994, 2021.

Tomczak, M.: Some historical, theoretical and applied aspects of quantitative water mass analysis, J. Mar. Res., 57, 275–303, https://doi.org/10.1357/002224099321618227, 1999.

Tomczak, M. and Large, D. G.: Optimum multiparameter analysis of mixing in the thermocline of the eastern Indian Ocean, J. Geophys. Res. Oceans, 94, 16141–16149, 1989.

Turnewitsch, R., Falahat, S., Stehlikova, J., Oguri, K., Glud, R. N., Middelboe, M., Kitazato, H., Wenzhöfer, F., Ando, K., Fujio, S., and Yanagimoto, D.: Recent sediment dynamics in hadal trenches: Evidence for the influence of higher-frequency (tidal, near-inertial) fluid dynamics, Deep Sea Res. Part Oceanogr. Res. Pap., 90, 125–138, https://doi.org/10.1016/j.dsr.2014.05.005, 2014.

Wang, F., Zhang, L., Hu, D., Wang, Q., Zhai, F., and Hu, S.: The vertical structure and variability of the western boundary currents east of the Philippines: case study from in situ observations from December 2010 to August 2014, J. Oceanogr., 73, 743–758, https://doi.org/10.1007/s10872-017-0429-x, 2017.

Wang, W., Köhl, A., and Stammer, D.: The deep meridional overturning circulation in the Indian Ocean inferred from the GECCO synthesis, Dyn. Atmospheres Oceans, 58, 44–61, https://doi.org/10.1016/j.dynatmoce.2012.08.001, 2012.

Warren, B. A.: Deep circulation of the world ocean, in: Evolution of physical oceanography, edited by: Warren, B. A. and Wunsch, C., Massachusetts Institude of Technology, Boston, 6–40, 1981.

Warren, B. A. and Brechner Owens, W.: Some preliminary results concerning deep Northern-Boundary currents in the North Pacific, Prog. Oceanogr., 14, 537–551, https://doi.org/10.1016/0079-6611(85)90027-8, 1985.

Watling, L., Guinotte, J., Clark, M. R., and Smith, C. R.: A proposed biogeography of the deep ocean floor, Prog. Oceanogr., 111, 91–112, https://doi.org/10.1016/j.pocean.2012.11.003, 2013.

Webb, T. J., Vanden Berghe, E., and O'Dor, R.: Biodiversity's big wet secret: The global distribution of marine biological records reveals chronic under-exploration of the deep pelagic ocean, PLoS ONE, 5, https://doi.org/10.1371/journal.pone.0010223, 2010.

Weston, J. J. and Jamieson, A. J.: The Multi-Ocean Distribution of the Hadal Amphipod, Hirondellea dubia (Crustacea, Amphipoda), Front. Mar. Sci., 9, 824640, 2022.

Wijffels, S. E., Hall, M. M., Joyce, T., Torres, D. J., Hacker, P., and Firing, E.: Multiple deep gyres of the western North Pacific: A WOCE section along 149°E, J. Geophys. Res. Oceans, 103, 12985–13009, https://doi.org/10.1029/98JC01016, 1998.

Wijffels, S. E., Sprintall, J., Fieux, M., and Bray, N.: The JADE and WOCE I10/IR6 throughflow sections in the southeast Indian Ocean. Part 1: Water mass distribution and variability, Deep Sea Res. Part II Top. Stud. Oceanogr., 49, 1341–1362, 2002.

Wust, G.: Thermometric Measurement of Depth, Int. Hydrogr. Rev., 28–49, 1933.

Zhai, F. and Gu, Y.: Abyssal Circulation in the Philippine Sea, J. Ocean Univ. China, 19, 249–262, https://doi.org/10.1007/s11802-020-4241-7, 2020.

Zhang, L. and Delworth, T.: Impact of the Antarctic bottom water formation on the Weddell Gyre and its northward propagation characteristics in GFDL CM2.1 model, J. Geophys. Res. Oceans, 121, 5825–5846, https://doi.org/10.1002/2016JC011790, 2016.

Zhou, C., Xu, H., Xiao, X., Zhao, W., Yang, J., Yang, Q., Jiang, H., Xie, Q., Long, T., Wang, T., Huang, X., Zhang, Z., Guan, S., and Tian, J.: Intense Abyssal Flow Through the Yap-Mariana Junction in the Western North Pacific, Geophys. Res. Lett., 49, https://doi.org/10.1029/2021GL096530, 2022.

Zhou, S., Meijers, A. J. S., Meredith, M. P., Abrahamsen, E. P., Holland, P. R., Silvano, A., Sallée, J.-B., and Østerhus, S.: Slowdown of Antarctic Bottom Water export driven by climatic wind and sea-ice changes, Nat. Clim. Change, 1–9, https://doi.org/10.1038/s41558-023-01695-4, 2023.

Zilberman, N., Roemmich, D., and Gilson, J.: Deep-ocean circulation in the Southwest Pacific Ocean interior: Estimates of the mean flow and variability using Deep Argo data, Geophys. Res. Lett., 47, e2020GL088342, 2020.